NEW TECHNIQUES IN SINGLE MOLECULE OPTICAL TRAPPING: PASSIVE TORQUE WRENCH WITH A SINGLE BEAM OPTICAL TRAP AND DNA Y STRUCTURE AS A VERSATILE, MULTIDIMENSIONAL SINGLE MOLECULE ASSAY

A Dissertation

Presented to the Faculty of the Graduate School

of Cornell University

In Partial Fulfillment of the Requirements for the Degree of

Doctor of Philosophy

by

James Inman

May 2014

NEW TECHNIQUES IN SINGLE MOLECULE OPTICAL TRAPPING: PASSIVE TORQUE WRENCH WITH A SINGLE BEAM OPTICAL TRAP AND DNA Y STRUCTURE AS A VERSATILE, MULTIDIMENSIONAL SINGLE MOLECULE ASSAY

James Inman, Ph. D.

Cornell University 2014

Optical trapping is a powerful single molecule technique used to study dynamic biomolecular events, especially those involving DNA and DNA-binding proteins. The optical trap has the capability to stretch, twist, or unzip single DNA molecules, usually along a single dimension. Access to more dimensions of a single molecule system will be an essential feature in next generation single molecule tools to study more complex bimolecular systems, such as transcription and replication machinery, that stretch, twist, and unwind multiple strands of DNA. To this end, two new techniques for single molecule optical trapping are presented. First, a passive torque wrench is developed to increase the versatility and flexibility of the angular optical trapping technique by passively clamping the toque while simultaneously monitoring the angular orientation of the trapped particle. Second, a novel optical trapping assay is presented that allows simultaneous DNA stretching, twisting, unzipping, and fluorescence of a three-branch DNA construct, the DNA Y structure.

BIOGRAPHICAL SKETCH

James Inman was born on April 4, 1985 in Los Angeles, CA. He attended Stone Bridge High School, VA from which he graduated with an advanced diploma. He enrolled at Radford University in fall of 2003 as a physics major with the intent of studying engineering. Instead he studied the fundamentals of physics, math, and chemistry. He graduated from Radford University summa cum laude with a Bachelor of Science in physics and Bachelor of Science in mathematics in 2007. A summer of research at Cornell in the NSF Research Experience for Undergraduates in the summer of 2006 inspired him to pursue a career in research. He began studies at Cornell in fall of 2007 in the physics PhD program. He joined the Wang lab to focus his knowledge of physics on the problems of biophysics. He completed a Master of Science in physics in the fall of 2011. He graduated from Cornell in May 2014with a Doctorate of Philosophy in physics.

To my wife, Elizabeth, and my son, Charles

ACKNOWLEDGMENTS

I would like to acknowledge my advisor Michelle D. Wang for her genuine interest in my success both academically and personally. Michelle's unwavering support enabled me to achieve my goals and see my projects to fruition. I would also like to thank my special committee members, James P. Sethna, and Mukund Vengalattore, for their feedback and contributions to my work.

I would like to thank the members of the Wang Lab who took time to introduce me to the optical trapping instruments and biological methods used in the lab: Daniel Johnson, Scott Forth, Jing Jin, Benjamin Smith, Michael Hall, and Maxim Sheinin. I would like to give special thanks to Bob Forties for many helpful discussions and generous assistance to my research. Last, I would like to thank all of the members of the Wang lab. The collaborative spirit of the lab has assisted me immensely over the years.

I would like to give thanks to all of the educators in my life who sparked my interest in higher education. I would like to give special thanks to my undergraduate professors and mentors Walter Jaronski, Rhett Herman, and Brett Taylor for their inspiring lectures, for engaging me in research, and providing the foundation for my graduate studies.

I would like to thank my parents Thomas and Patricia Inman for their unrelenting determination to see me succeed. They instilled into me the can do attitude and desire to achieve that drives me. Most of all, I would like to thank my wife Elizabeth Inman for her unconditional love and support. Without her daily encouragement and devotion to my happiness I would not have completed this work.

TABLE OF CONTENTS

LIST OF FIGURES

CHAPTER 1

OPTICAL TRAPPING AS A SINGLE MOLECULE TECHNIQUE

Introduction

Single molecule biophysics has greatly expanded our knowledge about the way in which proteins and DNA interact and function (Greenleaf et al. 2007; Moffitt et al. 2008; Forth et al. 2013). Studying single molecules in biology is necessary to measure fast asynchronous behaviors of proteins. Standard biochemical methods provide a vast foundation for understanding protein function; however, biochemical methods cannot provide manipulation to probe directly how forces and torques limit or alter the behavior of proteins. Furthermore, biochemical methods always measure and ensemble average of many proteins often undergoing many rounds of reactions. Therefore we use single molecule methods to distinguish the mechanical properties of single proteins undergoing single reaction cycles to understand and quantify their reaction pathways.

The Wang lab has pioneered new techniques in single molecule biophysics. Our lab focuses on the use of optical trapping and a DNA centric assay to measure the actions of single proteins interacting with DNA (Yin et al. 1995; Wang et al. 1997; Wang et al. 1998). The optical trap exerts forces and extends single DNA tethers via a trapped handle particle to detect the interaction of proteins with nanometer and piconewton precision. We have developed DNA unzipping as a method to probe the precise location and strength of interactions of proteins with DNA (Koch et al. 2002). We pioneered the angular optical trap which allowed for the application of twist and torque to the DNA (La Porta and Wang 2004). In this dissertation I will describe my

contributions to the development of novel single molecule optical trapping techniques. Specifically, a method for a passive torque wrench with the angular optical trap and a new assay which allows for a combination DNA stretching, twisting, and unzipping. This chapter will introduce the methods of stretching, twisting, and unzipping DNA used in single molecule optical trapping and motivate the need for more advanced techniques.

Manipulation of single molecules

Single molecule techniques observe and/or manipulate one molecule at a time. Optical tweezers achieve this feat by attaching a biological molecule to a handle particle such as a microsphere. The DNA centric assay involves attaching a single DNA molecule between the surface and the handle particle. To make measurements on a biological system, the handle particle is manipulated by the optical trap.

Stretching

This first and simplest single molecule assay is DNA stretching (**figure 1a**). The measured quantities are the end to end distance of the DNA and the total force on the tethered DNA. A surprising amount of information can be determined by such a simple assay.

The first task in using a DNA centric assay to study single molecule biology is to understand the behavior of dsDNA and ssDNA under force. Single molecule optical

tweezers experiments stretch DNA measure the force extension curves (Smith et al. 1996; Wang et al. 1997). These studies can be compared to theoretical work that applies statistical mechanics to describe DNA. Single stranded DNA is well described by a simple freely jointed chain polymer model (Smith et al. 1996); however, under low force the bases of the ssDNA can interact with each other forming secondary structure. The structural properties of double stranded DNA are well described by a worm like chain model. Experimental results have been well fit by several approximate solutions for the force extension relationship for low force where entropy dominates, for higher forces where enthalpy dominates, and more complete theories that combine both low and high force (Wang et al. 1997) or include contributions from the DNA's helical structure (Sheinin and Wang 2009). These measurements and the accompanying theoretical models are essential for interpreting single molecule measurements of protein-DNA interactions in the DNA centric assay.

Protein complexes bound to DNA can be detected by the stretching assay since they change the physical properties of the DNA. Protein complexes that bind DNA can be disrupted by force. This disruption is detected by the release of DNA from the protein surface or protein complex (**figure 1b**). Such disruption assays have been used to study the stability of the nucleosome arrays as well as single nucleosomes (Brower-Toland et al. 2002; Brower-Toland and Wang 2004). The stability of the protein-DNA complex can be estimated from the measured disruption force; however, discrimination of multiple proteins on a single tether is difficult.

DNA stretching is also useful for understanding the formation of protein filaments where many proteins bind to the DNA tether. Tension applied to the DNA tether alters the binding affinity of proteins. This rate of assembly or disassembly of protein filaments under force can be exploited to determine their molecular mechanism. A single molecule stretching study of RAD51, a key player in the initiation of homologous recombination, was able to determine that the filament disassembled one monomer at a time and that the filament must unravel from its ends (van Mameren et al. 2009). Another study revealed the mechanism of RecA, another protein responsible for initiating homologous recombination during DNA break repair, did not function under tension which implied that the 3D conformational dynamics of DNA is essential for the protein function (Forget and Kowalczykowski 2012). Thus, through modifying the DNA landscape by applying force a great deal can be learned about the mechanism of protein-DNA interactions.

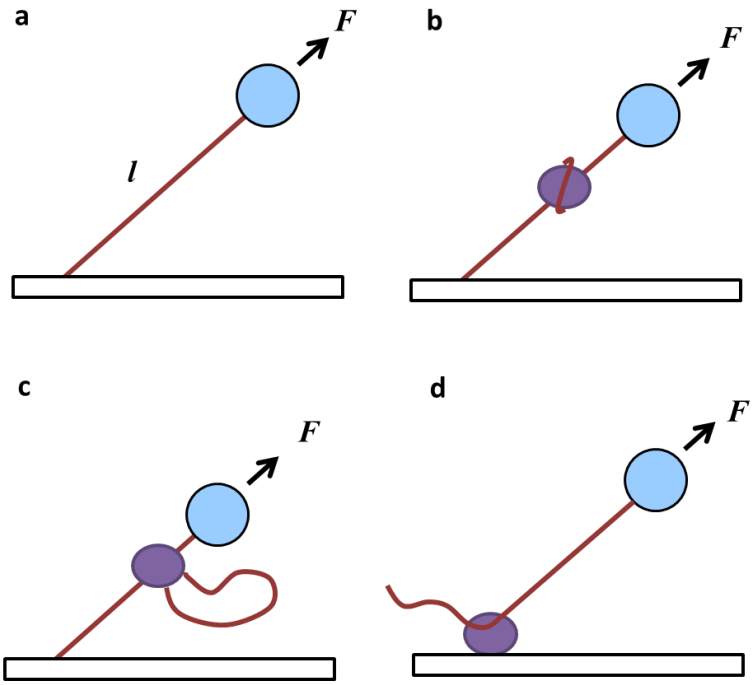

Figure 1. DNA centric single molecule measurement configurations. (**a**) A single DNA molecule is attached to a microscope cover glass at one end and a plastic microsphere at the other. By controlling the position of the microsphere and applied optical force, the end to end length (extension) and the force on the DNA is measured and manipulated. (**b**) Stretching the DNA tether can disrupt DNA-protein interactions. The force at which the disruption occurs as well as the accompanying change in DNA extension characterizes the interaction. (**c**) Proteins which actively create loops of DNA can be measured with the stretching assay because they change the amount of extended DNA. The processivity and frequency of events can be determined under varying forces. (**d**) Using a processive motor protein as the linkage of one end of the DNA tether, the velocity, step size, and processivity of molecular motors can be quantitatively determined as a function of resisting or assisting force.

Stretching DNA can also detect the dynamics of single proteins which alter the end to end length of DNA (**figure 1c**). Chromatin remodelers form loops of DNA between DNA binding domain and a translocation motor domain. Stretching assays have found that chromatin remodelers such as SWI/SNF and RSC are processive motors. They reel in large loops of DNA which are subsequently released in a sudden event. The stretching assay is ideal for measuring such looping activity, however, stretching alone cannot identify where the protein is located on the tether and it is challenging to be certain there is only a single protein acting on the DNA.

A variation of the stretching technique allows for the tracking of protein motors that move processively along DNA. Instead of the DNA strand being directly anchored, this assay holds the processive motor protein that is bound to the DNA tether (**figure 1d**). As the motor translocates on the DNA, it reels in the DNA strand. This type of assay measures the dynamics of a single protein that translocates along DNA such as the powerful molecular motor RNA polymerase (Yin et al. 1995; Wang et al. 1998). Such studies provide a wealth of knowledge about the processivity, maximum force generation, and even the kinetics of molecular motors (Bai et al. 2004; Shundrovsky et al. 2004). This technique requires the protein to be modified and attached directly to a surface which could alter its function. Additionally, all the proteins will begin to move at the same time so that only one or at best a few molecules can be observed in each sample chamber.

The next generation of stretching techniques is incorporating more complex DNA templates and measurement dimensions. One interesting new method used multiple traps to detect the location of bound proteins on one strand of DNA held with between two traps with another strand of DNA held between another set of traps (Noom et al. 2007). This new assay used a tightly stretched DNA strand as a sensor, like a violin string being plucked. Using a similar method, the strength of interaction between two strands of DNA bridged by H-NS protein was quantified (Dame et al. 2006). By using multiple optical traps, these studies manipulate multiple degrees of freedom and multiple DNA tethers to observe more complex biological systems.

Twising

The double helical nature of the DNA structure makes it so twist cannot be resolved when the DNA ends are torsionally constrained. Twisting leads to build up of torque in the DNA, like a torsional spring. This makes the twist and torque relevant to proteins that bind, constrain, or translocate along DNA (Koster et al. 2010; Forth et al. 2013).

To twist biomolecules, the optical trap must be enhanced to allow the rotation of the trapped particle. The polarized Gaussian trapping laser is capable of orienting and rotating an optically anisotropic particle (Friese et al. 1998). Our lab has pioneered the angular optical trap (AOT) to investigate rotational motions of biological molecules (La Porta and Wang 2004; Deufel et al. 2007). To achieve this, the

convention optical trap must be enhanced to include an anisotropic trapping particle, control of the input laser polarization, and direct detection of the torque applied by the trap (**figure 2**).

The trapping particle is optically birefringent nanofabricated quartz cylinder (**figure 2a**) (Deufel et al. 2007). The geometry of the cylinder orients it vertically with the long axis parallel to the trapping beam. The cylinder is functionalized only on its bottom so that biological molecules will be attached in a way that naturally allows rotation. The positive optical birefringence of quartz allows the cylinder to be aligned with the electric field of the linearly polarized trapping laser such that it can be rotated by rotation of the polarization. Thus the trapping particle is confined in all degrees of freedom and specifically functionalized for attachment to biomolecules.

The polarization of the trapping laser must be rapidly, flexibly, and accurately controlled. This is achieved by an interferometer in which the phase of the beam in each arm is modulated by an acousto-optic modulator (La Porta and Wang 2004). The beams are recombined and sent through a quarter wave plate in such a way that the phase difference is mapped into a rotation of the polarization. In this was the polarization direction of the trap can be modulated at ~100 kHz rates with ~urad resolution. This provides the level of polarization control needed to rotate the cylinder, actively feedback on the polarization to maintain a constant torque, or rapidly rotate the polarization in a passive torque clamp (see chapter 2).

Last, the torque exerted on the cylinder is directly measured by the forward scattered trapping beam (**figure 2b**) (Bishop et al. 2003; La Porta and Wang 2004). The cylinder will align its more polarizable axis with the trap's linear polarization to minimize the energy of the system. If the cylinder is not aligned in this way, there will be a restoring torque due to the misalignment of the induced dipole and the electric field. Such a torque will change the net angular momentum of the scattered trapping beam. By measuring the intensity of the right and left hand circular polarization outgoing beam, the optical torque exerted on the cylinder is measured directly.

In addition to stretching, DNA can be twisted and one can explore the rich phase behavior of DNA under twist and torque. Although the canonical B-form DNA structure is the most prevalent in nature, other structural forms are known to have an important role in biological processes. Having the capability to exert twist and measure torque allows unambiguous characterization of the various phase transitions of DNA. Winding of the DNA under a constant force, the extension and torque of the DNA is measured to give clear indication of the beginning and end of phase transitions. Using this technique, the angular optical trap has been able to map out the boundaries between several DNA phases as well as the physical properties which characterize these states (Forth et al. 2008; Daniels et al. 2009; Sheinin and Wang 2009; Sheinin et al. 2011).

Twist and torque not only affect the state of the DNA molecule, but also how proteins interact with DNA. Our lab has used an angular optical trap to demonstrate the

influence that torque has on DNA-protein interactions. Nucleosome stability is altered under torque and there is a loss of histones when a nucleosome is disrupted by stretching under torque (Sheinin et al. 2013). The powerful molecular motor RNA polymerase can generate a torque large enough to melt DNA and alter the nucleosome structure (Ma et al. 2013). In these experiments, the angle of the handle particle is controlled while the torque is measured. In contrast, a passive torque clamp imposes a constant torque on the handle particle without active feedback while the angle of the handle is measured (**chapter 2**) (Inman et al. 2010). Having full control of either twist or torque during an experiment will be vital to fully characterizing how proteins move on and interact with DNA.

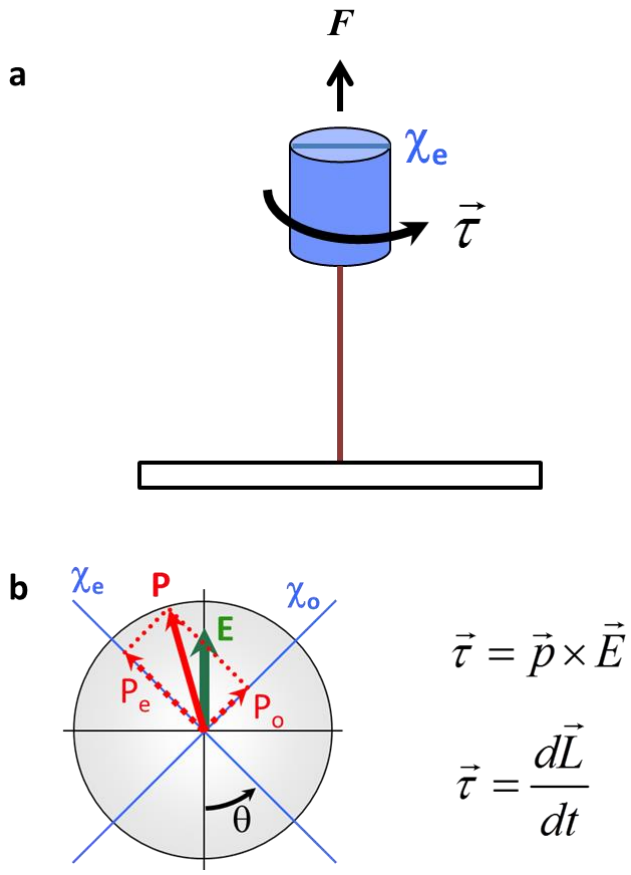

Figure 2. Twisting DNA with and angular optical trap. (**a**) Cartoon depicting the configuration of the angular optical trap. A single DNA tether is torsionally constrained to a microscope coverslip via multiple attachment points. The other end is also torsionally constrained to a quartz cylinder held in an optical trap. The tether should only be stretched along the z-axis such that the cylinder axis remains aligned with laser beam propagation. (**b**) The particle is angularly trapped by linearly polarized light. Deviations from this trapping minimum result in an optical torque due to a misalignment of the electric field and the induced polarization of the birefringent

quartz nanofabricated cylinder. The optical torque exerted on the cylinder can be directly determined by the change in angular momentum of the laser beam.

Unzipping

Stretching and twisting will tend to destabilize the base-pairing interactions that hold the two strands of DNA together. By pulling on the two strands of DNA, the dsDNA can be mechanically unwound (unzipped) into two ssDNA molecules (**figure 3a**) (Bockelmann et al. 1997; Essevaz-Roulet et al. 1997). As a DNA molecule is unzipped, proteins bound to the DNA are disrupted and their presence can be detected by the unzipping fork. This results in a unique method for scanning a DNA template to detect the location and the strength of interaction of proteins (Koch et al. 2002; Koch and Wang 2003).

In the absence of any binding proteins, the force required to unzip DNA varies about a mean force. Due to the non-uniform base pairing and base stacking interactions, the force required to unzip DNA is modulated by the underlying DNA sequence. It takes more force to disrupt the stronger G-C base pair than the weaker A-T base pair and the additional stacking interactions between neighboring base-pairs also contribute to variations. Using the nearest neighbor model for base pairing and stacking interactions from thermodynamic studies, the unzipping force can be predicted reasonably well using a simple statistical mechanical model (Bockelmann et al. 1998). Alternatively, the measured force can be used to fit the parameters of the nearest neighbor model (Huguet et al. 2010). In this way, unzipping protein free DNA provides the force baseline for detecting protein-DNA interactions. Additionally, as the DNA is unzipped the force and extension of the tether, together with the

theoretical models of dsDNA and ssDNA, are used to calculate the number of base pairs which have been separated. Taken together, the force and number of base pairs unzipped provide information about the strength and location of interactions.

Unzipping DNA through a bound protein can provide detailed information about strengths and locations of individual protein-DNA interactions because these interactions tend to stabilize the DNA duplex. When the fork encounters such stabilized DNA, more force will be required to disrupt the DNA and/or DNA protein interactions. This force rise can accurately and precisely measure the locations of a bound proteins on DNA (Koch et al. 2002; Koch and Wang 2003; Shundrovsky et al. 2006). Moreover, analysis of the force peaks by dynamic force spectroscopy determine the strengths of multiple interactions within a protein-DNA complex. This technique has been used to map out the detailed interactions of DNA with a nucleosome and analyze the strengths of those interactions (Hall et al. 2009; Forties et al. 2011). Importantly, this technique is sensitive enough to detect changes in the affinity histone variants (Dechassa et al. 2011). Thus, the unzipping technique provides a powerful and precise way to map out protein-DNA interactions.

Figure 3. Unzipping of DNA to detect the location and strength of interactions of bound proteins. (**a**) DNA is mechanically separated from dsDNA into two strands of ssDNA (unzipped) by applying force to opposite strands of a dsDNA molecule. Using theoretical models of dsDNA and ssDNA the force and extension of the extended DNA is used to calculate the number of basepairs unzipped j. (**b**) Bound proteins stabilize the unzipping fork and result in an increase in the force at the location j_{protein}. The force required to disrupt the protein-DNA complex characterizes the strength of protein-DNA interaction. (**c**) Unzipping DNA resembles a replication fork and is a powerful technique for studying proteins that work on forked DNA such as replicative helicases. A force applied to the extended DNA assists the helicase as it unwinds DNA.

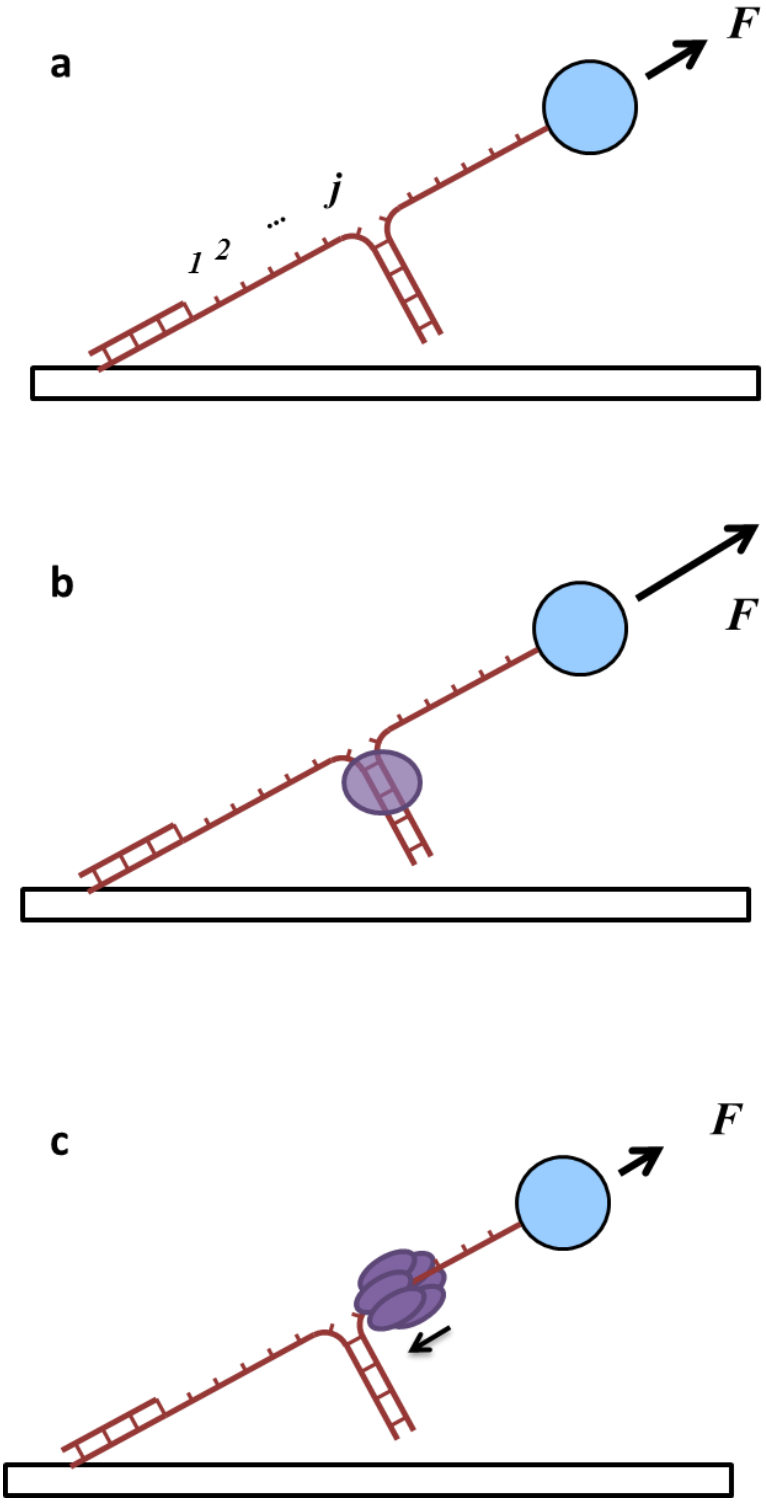
a
F
j
...
1
2
b
F
c
F

As DNA is unzipped, long segments of single strand DNA (ssDNA) are generated. This provides a ssDNA template to study the many proteins which bind to and translocate on ssDNA during DNA replication, recombination, and repair. Proteins which work at the fork such as replicative helicases and polymerases can be tracked with this assay (**figure 3c**). The ability to track and apply an assisting force to the opening of dsDNA by the t7 helicase has led to important discoveries of non-processive motion such as slippage which can only be observed at the single molecule level (Johnson et al. 2007; Sun et al. 2011). While the unzipping of DNA can provide a long ssDNA template under force, a drawback of this technique is that the DNA will spontaneously reanneal if the force is lowered.

DNA unzipping is a versatile single molecule technique to locate, probe interaction strength, and track proteins on DNA. However, current techniques to unzip DNA cannot manipulate the DNA downstream of the unzipping fork since it is not constrained (**figure 3a**). This precludes the use of stretching and twisting techniques on the unzipping DNA template.

Combination of multiple techniques

While each of the three single molecule techniques have many strengths on their own, combining them together would open new possibilities and be capable of discerning more clearly the outcomes of biological events. Stretching and twisting are already achieved simultaneously by the angular optical trap (Deufel et al. 2007; Forth et al.

2008). However, combining all three methods together simultaneously or sequentially has not been possible. Unzipping DNA simultaneously with stretching or twisting will allow experiments to explore how DNA protein interactions are perturbed by force and torque. By combining the techniques sequentially on same DNA tether, first a DNA stretching or twisting experiment measures the dynamics of protein events, such as those described above, and then the DNA is unzipped to take a snapshot of the proteins on the DNA, mapping out the detailed location and strengths of protein interactions.

Also, new single molecule manipulation techniques should be compatible with fluorescence. The combination of optical trapping and fluorescence has been successful in resolving important biological questions by collecting more information about what is present on the DNA. While fluorescence does not increase the degrees of manipulation of the system, new degrees of observation are only limited by the number of colors that can be observed simultaneously. To be compatible with fluorescence, the template DNA should be extended in the imaging plane of the microscope. In this way, stretching techniques are already compatible with fluorescence (Wang et al. 1997), however, twisting and unzipping DNA are not. The angular optical trap must stretch the tether along the axis of the trapping laser such that the DNA is perpendicular to the trapping plane (Deufel and Wang 2006; Deufel et al. 2007); and during unzipping the DNA template which is to be unzipped is not extended at all (Koch et al. 2002).

Dissertation Outline

This dissertation focuses on the development of new techniques in single molecule optical trapping. Access to more dimensions of a single molecule system will be an essential feature in next generation single molecule tools to aid in unraveling the mechanisms of *in vitro* biological systems of ever increasing complexity as we work towards duplicating *in vivo* processes. To this end, the Wang lab continues to develop novel single molecule tools. This dissertation is a collection of two novel single molecule techniques: the first is a passive optical torque wrench and the second is the DNA Y structure.

The passive optical torque wrench is an extension of the angular optical trap developed in the Wang lab to twist and torque biomolecules. The angular optical trap is particularly well suited to confine a trapped particle's angular orientation and simultaneously measure the optical torque required to do so (La Porta and Wang 2004). The conjugate of this process is more difficult to achieve. In principle it is possible to feedback on the torque signal of the angular optical trap in an active torque clamp (La Porta and Wang 2004); however, this is impractical for biological systems which stall before producing torques disguisable from the noise, on the order of tens of pN*nm of torque (Ma et al. 2013). Chapter 2 describes and demonstrates a method for generating a passive torque wrench with an optical trap. This extension to the standard angular optical trap exerts a constant torque on the trapped particle while

simultaneously measuring the angular orientation of the particle. A distinct advantage of this method is that the instrument can be rapidly switched between the two modes of trapping. To demonstrate this technique, a DNA tether is over twisted in the angular trap mode and then allowed to unwind in the passive torque wrench mode.

Chapter 3 describes a new single molecule technique that combines DNA stretching, twisting, and unzipping. The DNA Y structure is a three way junction of DNA which is constrained at each of its three ends by dual optical traps and the surface of the microscope slide. By pulling on all three strands of DNA the forces and extensions of each strand can be determined simultaneously. Furthermore, twist can be introduced by winding the DNA with the optical traps. Finally, one segment of the Y structure can be unzipped while concurrently being stretched and twisted. This assay is also shown to be compatible with fluorescence microscopy which further increases its versatility. This new single molecule technique synergistically combines the strengths of existing assays to be applied concurrently or sequentially to biological molecules.

References

Bai, L., Shundrovsky, A. and Wang, M. D. (2004). "Sequence-dependent kinetic model for transcription elongation by RNA polymerase." J Mol Biol **344**(2): 335-349.

Bishop, A. I., Nieminen, T. A., Heckenberg, N. R. and Rubinsztein-Dunlop, H. (2003). "Optical application and measurement of torque on microparticles of isotropic nonabsorbing material." Physical Review A **68**(3).

Bockelmann, U., Essevaz-Roulet, B. and Heslot, F. (1998). "DNA strand separation studied by single molecule force measurements." Physical Review E **58**(2): 2386-2394.

Bockelmann, U., EssevazRoulet, B. and Heslot, F. (1997). "Molecular stick-slip motion revealed by opening DNA with piconewton forces." Physical Review Letters **79**(22): 4489-4492.

Brower-Toland, B. and Wang, M. D. (2004). "Use of optical trapping techniques to study single-nucleosome dynamics." Methods Enzymol **376**: 62-72.

Brower-Toland, B. D., Smith, C. L., Yeh, R. C., Lis, J. T., Peterson, C. L. and Wang, M. D. (2002). "Mechanical disruption of individual nucleosomes reveals a reversible multistage release of DNA." Proc Natl Acad Sci U S A **99**(4): 1960-1965.

Dame, R. T., Noom, M. C. and Wuite, G. J. (2006). "Bacterial chromatin organization by H-NS protein unravelled using dual DNA manipulation." Nature **444**(7117): 387-390.

Daniels, B. C., Forth, S., Sheinin, M. Y., Wang, M. D. and Sethna, J. P. (2009). "Discontinuities at the DNA supercoiling transition." Phys Rev E Stat Nonlin Soft Matter Phys **80**(4 Pt 1): 040901.

Dechassa, M. L., Wyns, K., Li, M., Hall, M. A., Wang, M. D. and Luger, K. (2011). "Structure and Scm3-mediated assembly of budding yeast centromeric nucleosomes." Nat Commun **2**: 313.

Deufel, C., Forth, S., Simmons, C. R., Dejgosha, S. and Wang, M. D. (2007). "Nanofabricated quartz cylinders for angular trapping: DNA supercoiling torque detection." Nat Methods **4**(3): 223-225.

Deufel, C. and Wang, M. D. (2006). "Detection of forces and displacements along the axial direction in an optical trap." Biophys J **90**(2): 657-667.

Essevaz-Roulet, B., Bockelmann, U. and Heslot, F. (1997). "Mechanical separation of the complementary strands of DNA." Proc Natl Acad Sci U S A **94**(22): 11935-11940.

Forget, A. L. and Kowalczykowski, S. C. (2012). "Single-molecule imaging of DNA pairing by RecA reveals a three-dimensional homology search." Nature **482**(7385): 423-427.

Forth, S., Deufel, C., Sheinin, M. Y., Daniels, B., Sethna, J. P. and Wang, M. D. (2008). "Abrupt buckling transition observed during the plectoneme formation of individual DNA molecules." Phys Rev Lett **100**(14): 148301.

Forth, S., Sheinin, M. Y., Inman, J. and Wang, M. D. (2013). "Torque measurement at the single-molecule level." Annu Rev Biophys **42**: 583-604.

Forties, R. A., North, J. A., Javaid, S., Tabbaa, O. P., Fishel, R., Poirier, M. G. and Bundschuh, R. (2011). "A quantitative model of nucleosome dynamics." Nucleic Acids Res **39**(19): 8306-8313.

Friese, M. E. J., Nieminen, T. A., Heckenberg, N. R. and Rubinsztein-Dunlop, H. (1998). "Optical alignment and spinning of laser-trapped microscopic particles." Nature **394**(6691): 348-350.

Greenleaf, W. J., Woodside, M. T. and Block, S. M. (2007). "High-resolution, single-molecule measurements of biomolecular motion." Annu Rev Biophys Biomol Struct **36**: 171-190.

Hall, M. A., Shundrovsky, A., Bai, L., Fulbright, R. M., Lis, J. T. and Wang, M. D. (2009). "High-resolution dynamic mapping of histone-DNA interactions in a nucleosome." Nat Struct Mol Biol **16**(2): 124-129.

Huguet, J. M., Bizarro, C. V., Forns, N., Smith, S. B., Bustamante, C. and Ritort, F. (2010). "Single-molecule derivation of salt dependent base-pair free energies in DNA." Proc Natl Acad Sci U S A **107**(35): 15431-15436.

Inman, J., Forth, S. and Wang, M. D. (2010). "Passive torque wrench and angular position detection using a single-beam optical trap." Opt Lett **35**(17): 2949-2951.

Johnson, D. S., Bai, L., Smith, B. Y., Patel, S. S. and Wang, M. D. (2007). "Single-molecule studies reveal dynamics of DNA unwinding by the ring-shaped T7 helicase." Cell **129**(7): 1299-1309.

Koch, S. J., Shundrovsky, A., Jantzen, B. C. and Wang, M. D. (2002). "Probing protein-DNA interactions by unzipping a single DNA double helix." Biophys J **83**(2): 1098-1105.

Koch, S. J. and Wang, M. D. (2003). "Dynamic force spectroscopy of protein-DNA interactions by unzipping DNA." Phys Rev Lett **91**(2): 028103.

Koster, D. A., Crut, A., Shuman, S., Bjornsti, M. A. and Dekker, N. H. (2010). "Cellular strategies for regulating DNA supercoiling: a single-molecule perspective." Cell **142**(4): 519-530.

La Porta, A. and Wang, M. D. (2004). "Optical torque wrench: angular trapping, rotation, and torque detection of quartz microparticles." Phys Rev Lett **92**(19): 190801.

Ma, J., Bai, L. and Wang, M. D. (2013). "Transcription under torsion." Science **340**(6140): 1580-1583.

Moffitt, J. R., Chemla, Y. R., Smith, S. B. and Bustamante, C. (2008). "Recent advances in optical tweezers." Annu Rev Biochem **77**: 205-228.

Noom, M. C., van den Broek, B., van Mameren, J. and Wuite, G. J. (2007). "Visualizing single DNA-bound proteins using DNA as a scanning probe." Nat Methods **4**(12): 1031-1036.

Sheinin, M. Y., Forth, S., Marko, J. F. and Wang, M. D. (2011). "Underwound DNA under tension: structure, elasticity, and sequence-dependent behaviors." Phys Rev Lett **107**(10): 108102.

Sheinin, M. Y., Li, M., Soltani, M., Luger, K. and Wang, M. D. (2013). "Torque modulates nucleosome stability and facilitates H2A/H2B dimer loss." Nat Commun **4**: 2579.

Sheinin, M. Y. and Wang, M. D. (2009). "Twist-stretch coupling and phase transition during DNA supercoiling." Phys Chem Chem Phys **11**(24): 4800-4803.

Shundrovsky, A., Santangelo, T. J., Roberts, J. W. and Wang, M. D. (2004). "A single-molecule technique to study sequence-dependent transcription pausing." Biophys J **87**(6): 3945-3953.

Shundrovsky, A., Smith, C. L., Lis, J. T., Peterson, C. L. and Wang, M. D. (2006). "Probing SWI/SNF remodeling of the nucleosome by unzipping single DNA molecules." Nat Struct Mol Biol **13**(6): 549-554.

Smith, S. B., Cui, Y. and Bustamante, C. (1996). "Overstretching B-DNA: the elastic response of individual double-stranded and single-stranded DNA molecules." Science **271**(5250): 795-799.

Sun, B., Johnson, D. S., Patel, G., Smith, B. Y., Pandey, M., Patel, S. S. and Wang, M. D. (2011). "ATP-induced helicase slippage reveals highly coordinated subunits." Nature **478**(7367): 132-135.

van Mameren, J., Modesti, M., Kanaar, R., Wyman, C., Peterman, E. J. and Wuite, G. J. (2009). "Counting RAD51 proteins disassembling from nucleoprotein filaments under tension." Nature **457**(7230): 745-748.

Wang, M. D., Schnitzer, M. J., Yin, H., Landick, R., Gelles, J. and Block, S. M. (1998). "Force and velocity measured for single molecules of RNA polymerase." Science **282**(5390): 902-907.

Wang, M. D., Yin, H., Landick, R., Gelles, J. and Block, S. M. (1997). "Stretching DNA with optical tweezers." Biophys J **72**(3): 1335-1346.

Yin, H., Wang, M. D., Svoboda, K., Landick, R., Block, S. M. and Gelles, J. (1995). "Transcription against an applied force." Science **270**(5242): 1653-1657.

CHAPTER 2

PASSIVE TORQUE WRENCH AND ANGULAR POSITION DETECTION USING A SINGLE BEAM OPTICAL TRAP

*Adapted from Optical Letters, Volume 35, Issue 17, pp. 2949-2951. Inman, J., Forth, S., and Wang. M.D. *Passive torque wrench and angular position detection using a single-beam optical trap*.

Introduction

The recent advent of angular optical trapping techniques has allowed for rotational control and direct torque measurement on biological substrates. Here we present a novel method that increases the versatility and flexibility of these techniques. We demonstrate that a single beam with a rapidly rotating linear polarization can be utilized to apply a constant controllable torque to a trapped particle without active feedback while simultaneously measuring the particle's angular position. In addition, this device can rapidly switch between a torque wrench and an angular trap. These features should make possible torsional measurements across a wide range of biological systems.

Optical trapping has proven to be an invaluable tool in the study of biophysical systems. The ability to measure the forces and displacements of nucleic acids, proteins, and molecular motors has allowed for further insight into the mechanistic functions of these important biological molecules (Wang et al. 1998; Bustamante et al. 2003). Recent advances in optical trapping techniques have led to methods by which rotational orientation and torque can also be manipulated and measured via the coupling of the polarization state of light to an optically or spatially anisotropic particle (Friese et al. 1998; Paterson et al. 2001; Galajda and Ormos 2003; La Porta and Wang 2004). We have previously developed such an angular optical trap and used it to measure the torsional properties of DNA (La Porta and Wang 2004; Deufel et al. 2007; Forth et al. 2008; Sheinin and Wang 2009).

In this work, we demonstrate a method to enhance the versatility of an angular optical trap. A constant optical torque may be exerted on a trapped particle without the need for active feedback or additional laser/optics to monitor the trapped particle's angular position using a single beam with a rapidly rotating linear polarization. This method is particularly well suited to exert torques relevant to single molecule biology experiments, ranging from near zero to several tens of pN nm. Such an instrument can be rapidly switched to a standard angular trapping mode. In comparison with previous work, this approach is unique in several aspects. The current torque wrench has little torque noise; whereas the optical torque wrench we developed earlier requires active feedback for torque stabilization (La Porta and Wang 2004) and thus the noise from Brownian motion can dominate for small torque values. Another study exerted torque using a similar method but requires the use of an additional laser/optics for the detection of the trapped particle's angular position. (Funk et al. 2009). A single circularly polarized beam can also provide a constant torque (Wood et al. 2008), but the magnitude of the torque is not controllable independently of the power of the trapping beam. In contrast, the current method provides a tunable constant torque without the need to change the laser power.

Method of passive torque wrench

The passive torque wrench is achieved by spinning the input linear polarization so rapidly that the particle cannot keep up with it. At this limit, the angular stiffness of the trapping beam approaches zero and it exerts an effectively constant torque on the particle in the direction of polarization rotation. The implementation of this method is outlined in **Fig.**

1(a). To understand this, consider a particle inside a trap with its polarization rotating at angular frequency $\omega = 2\pi f$. The equation of motion of the particle is:

$$\gamma \frac{d\theta}{dt} = \tau_0 \sin[2(\omega t - \theta)], \quad (1)$$

where γ is the rotational viscous damping coefficient and τ_0 is the maximum optical torque. This describes a damped-forced oscillator at low Reynold's number, where the viscous drag torque balances the optical torque. A similar description also characterizes optically torqued nanorods and magnetic particles (Bonin et al. 2002; McNaughton et al. 2007). Below a critical frequency $\omega_{\text{critical}} = 2\pi f_{\text{critical}} = \frac{\tau_0}{\gamma}$, the particle tracks the polarization rotation with a torque-dependent angular offset, resulting in a linear increase in the optical torque (La Porta and Wang 2004). However, above the critical frequency, the particle can no longer fully track the polarization and instead wobbles periodically in response to the polarization rotation. When $\omega >> \omega_{\text{critical}}$, although the trap exerts a full amplitude oscillating torque on the particle, the resulting wobble amplitude of the particle becomes diminishingly small as the particle simply can not respond faster than its corner frequency in a stationary angular trap ($\omega_{\text{corner}} = 2\omega_{\text{critical}}$). At this limit, the polarization effectively scans a quasi-stationary particle, and only a minute biased optical torque is exerted on the particle averaged over a cycle of the scan. In general, the mean torque τ may be obtained from Eq. (1) (Strogatz 1994): $\tau = \gamma\omega$ if $\omega \le \omega_{\text{critical}}$ and $\tau = \gamma\left(\omega - \sqrt{\omega^2 - (\tau_0/\gamma)^2}\right)$ if $\omega > \omega_{\text{critical}}$.

Detection of the angular position

First, we demonstrate the use of a lock-in method for detection of the angular position θ of the trapped particle. In general, θ can be determined from the input polarization angle and the torque signal (La Porta and Wang 2004), since the optical torque is $\tau(t) = \tau_0 \sin[2(\omega t - \theta)]$, where θ may be time-varying. In the limit of $\omega >> \omega_{\text{critical}}$, θ varies slowly compared to ω and its detection can be facilitated by a lock-in method. The reference signal is the intensity of the input beam polarized along the *x*-axis fixed in the lab frame $I_x(t) = I_0 \cos^2(\omega t) = I_0 [1 + \cos(2\omega t)]/2$ and the input signal is $\tau(t)$. Thus θ can be determined by the phase delay or time delay Δt output of the lock-in amplifier: $\theta = \omega \Delta t + \pi/4$ (**Fig. 1(b)**). In order to verify the lock-in method, we applied it to an irregularly shaped, micron-sized quartz particle so that the particle's angular position could be simultaneously recorded via video-tracking. As shown in **Fig. 1(c)**, the two methods agree to within the resolution of the video tracking method, and the particle underwent a slightly biased rotational diffusion. In practice, for ease of use, calibration, and reproducibility, the trapping particles are nanofabricated quartz cylinders which are uniform in size (~ 0.5 μm in diameter and ~ 1 μm in height), shape, and optical properties, and are functionalized on the bottom surface for specific attachment to biomolecules if desired (Deufel et al. 2007).

Figure 1: Method of constant optical torque generation and angular position detection. (a) Simplified schematic of the passive optical torque wrench. The optical setup is similar to what has been previously described (La Porta and Wang 2004) but with the important addition of a lock-in amplifier. (b) The lock-in amplifier uses $I_x(t)$ as reference signal and the torque detector signal $\tau(t)$ as the input signal. The phase difference between these two signals provides the angular position θ of the cylinder. (c) Comparison of detected angular position of a quartz dust particle as simultaneously determined by the lock-in method (red line) and video tracking method (blue points). For both (b) and (c), f_{critical} = 9 Hz and f = 1 kHz.

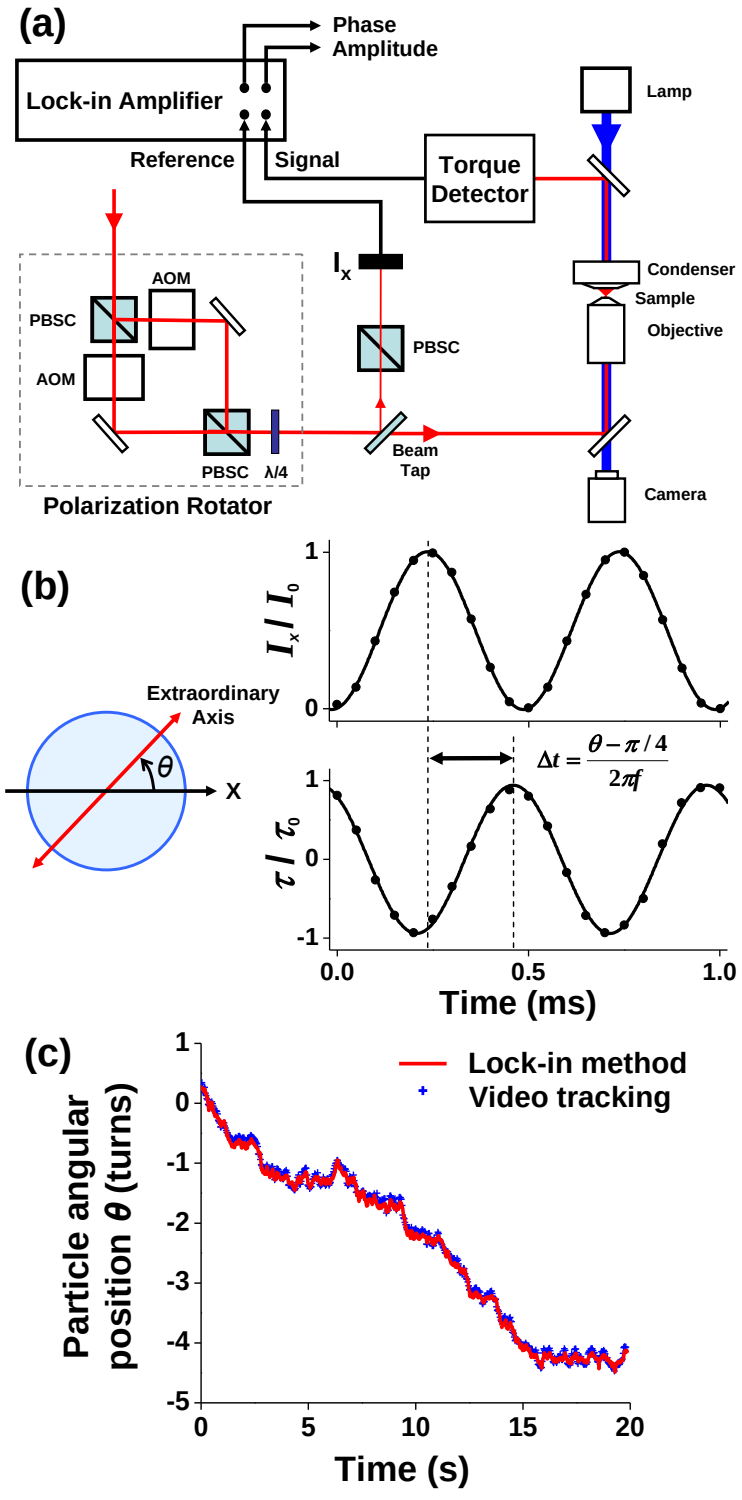
(a)
Phase
Amplitude
Lock-in Amplifier
Reference
Signal
Torque Detector
Lamp
Condenser
Sample
Objective
Camera
I_x
AOM
PBSC
AOM
PBSC
PBSC
λ/4
Beam Tap
Polarization Rotator
(b)
Extraordinary Axis
θ
X
I_x / I_0
τ / τ_0
$\Delta t = \frac{\theta - \pi/4}{2\pi f}$
1
0
-1
0.0
0.5
1.0
Time (ms)
(c)
Lock-in method
Video tracking
Particle angular position θ (turns)
1
0
-1
-2
-3
-4
-5
0
5
10
15
20
Time (s)

Demonstration of the passive torque wrench

Second, we demonstrate the use of this device as a passive torque wrench, with particular emphasis on the cases where $\omega >> \omega_{\text{critical}}$. **Fig. 2(a)** shows examples of the angular position of a single cylinder, tracked with the lock-in method, at different polarization rotation rates. Under a positive (negative) polarization rotation rate the cylinder underwent a small net positive (negative) rotation. This cylinder rotation rate (and thus the torque) decreased with an increase in the polarization rotation rate. At a given polarization rotation rate, the cylinder rotated smoothly, indicating a constant optical torque was exerted on the cylinder. The optical torque was directly measured by the torque detector (**bottom panel of Fig. 2(a)**) and was found to be consistent with the corresponding viscous torque calculated based on the cylinder rotation rate (**top panel of Fig. 2(a)**). **Fig. 2(b)** shows the mean torque on a single cylinder measured under a wide range of polarization rotation rates and laser powers. As expected, as ω was increased from zero, torque increased linearly as per the well-known Stokes' drag relation until $\omega = \omega_{\text{critical}}$, beyond which the torque decreases as expected. In addition, the torque magnitude scales with the trapping laser power. Therefore, to dial in a desired torque, either the polarization rotation rate or the laser power can be changed.

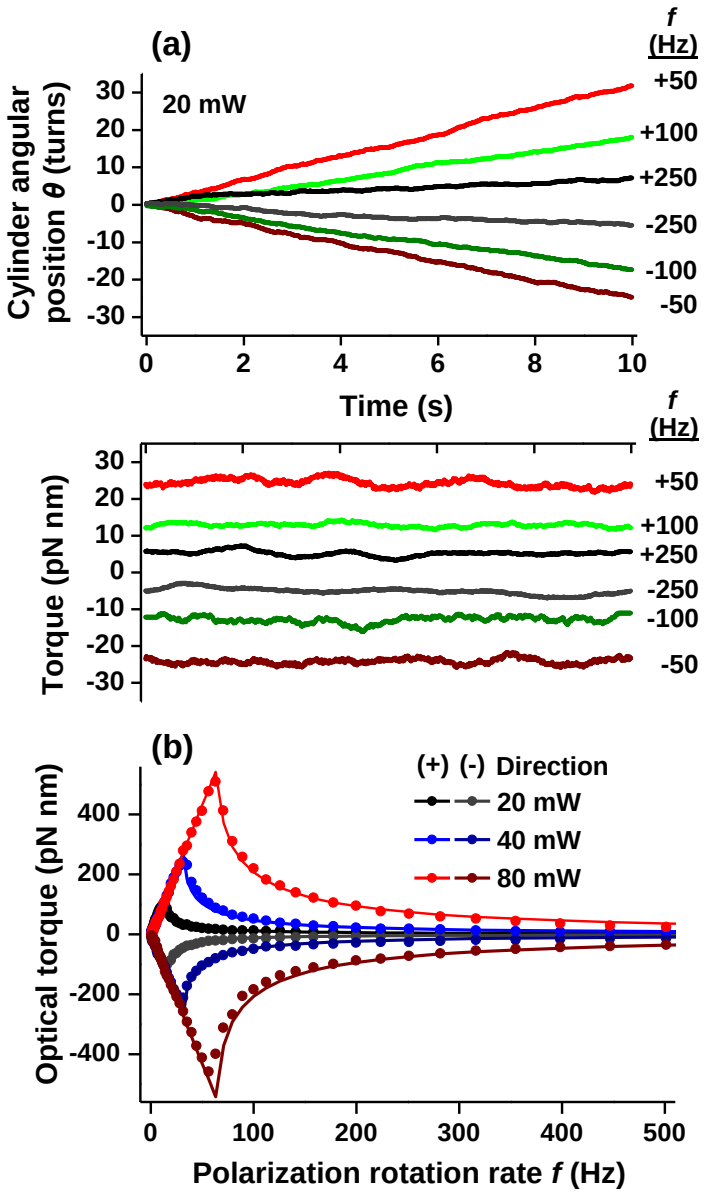

Figure 2: Demonstration of the passive torque wrench mode. (a) Single traces of cylinder angular position versus time for various polarization rotation rates and the corresponding measured torque. f_{critical} = 13 Hz. (b) Direct measurement of the torque versus polarization rotation rate for various laser powers on a quartz cylinder. Solid lines are global fits to the expected mean torque.

Rapid and smooth transition between traditional and passive torque wrench modes

Third, we show that this device can be switched rapidly between two useful operating modes. When $\omega < \omega_{\text{critical}}$, the cylinder is angularly trapped and tracks the rotation of the polarization. This mode should be used when a specific extent of cylinder rotation is desired. When $\omega >> \omega_{\text{critical}}$, the trap acts as a torque wrench. A constant torque is exerted on the cylinder while the angle of the cylinder is allowed to vary. We demonstrate this capability in **Fig. 3** by subjecting a cylinder to an angular trapping mode by slow (+) polarization rotation, switching to a passive torque wrench mode by rapid (+) polarization rotation , and then switching back to an angular trapping model by slow (–) polarization rotation. As shown, the cylinder underwent a constant rotation, followed by diffusive Brownian motion under a near zero torque condition, and then underwent a reverse rotation.

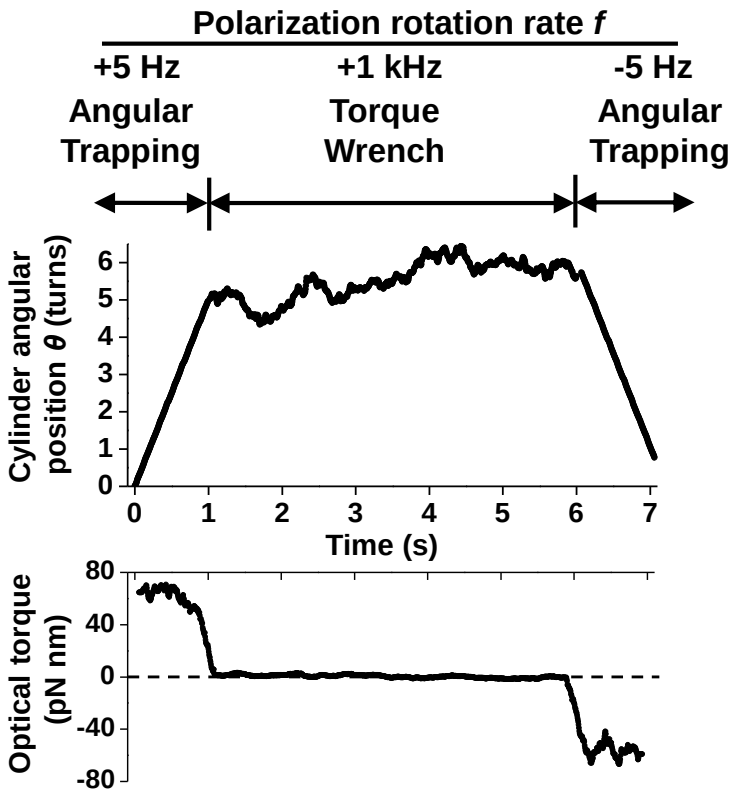

Figure 3: Demonstration of rapid switching between an angular trapping mode and a torque wrench mode. f_{critical} = 9 Hz. Polarization rate was set to +5 Hz at t = 0 (angular trapping mode), 1 kHz at t = 1 s (torque wrench mode), and –5 Hz at t = 6 s (angular trapping mode).

DNA unwinding with the passive torque wrench

Finally, we combine these features to observe DNA under torsion. A torsionally constrained DNA tether is formed by attaching a dsDNA to the microscope coverslip at one end and a quartz cylinder at the other (**Fig 4(a)**). The tether is over-twisted by rotating the cylinder by 15 turns in angular trapping mode under a constant force of 0.5 pN. Under this force and torque the DNA buckles to form plectonemes which can be detected by a decrease in the measured DNA extension (Forth et al. 2008; Daniels et al. 2009). The torsional stress in the DNA is released by entering the torque wrench mode set to near zero torque. **Fig 4(b)** shows the release of torsional stress in the DNA. As plectonemes are lost from the tether, the DNA extension increases until all plectonemes are lost and the tether extension plateaus at the expected number of basepairs (**top panel of Fig 4(b)**). The cylinder angle shows the full release of twist introduced to the tether (**bottom panel of Fig 5(b)**).

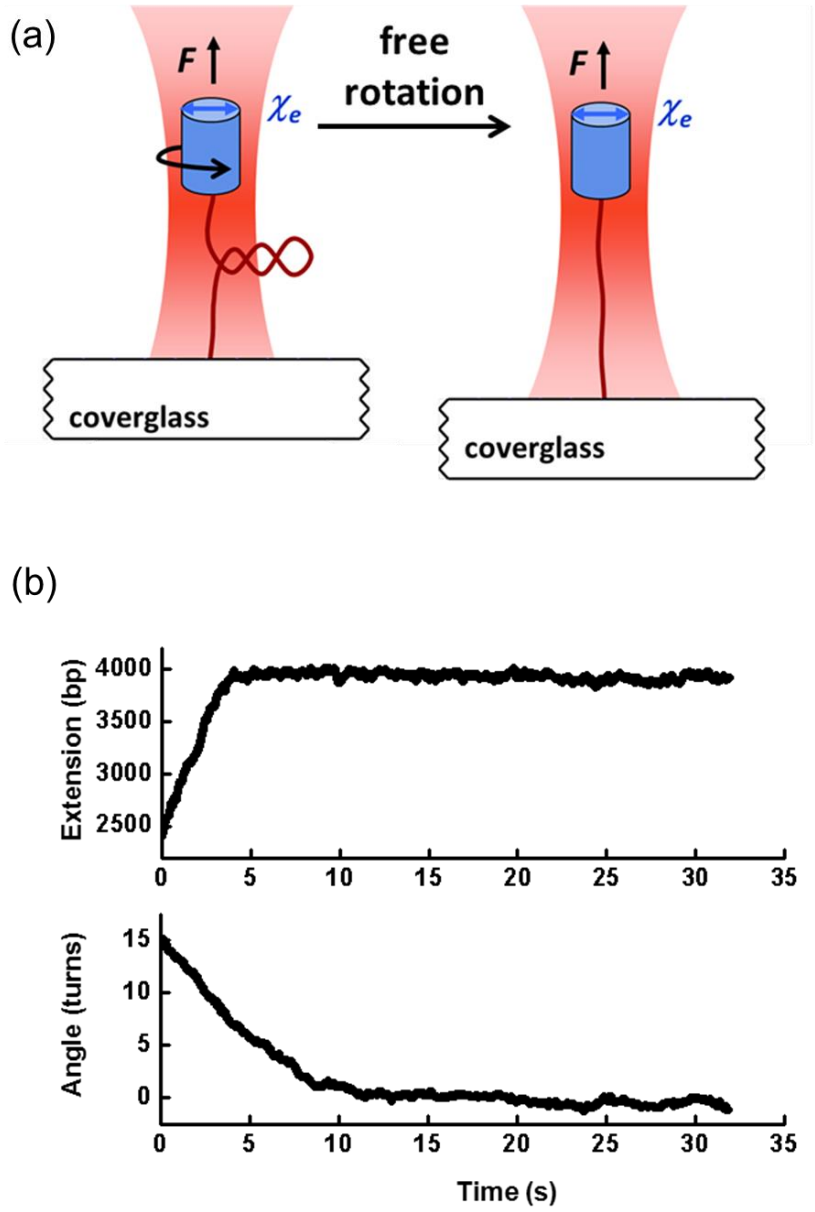

Figure 4: Torsional relaxation of DNA tether. (a) A schematic of the experimental setup with a torsionally contrained DNA tether. The DNA tether is initially over twisted using the angular trap mode. Then, the tether is allowed to freely rotate in passive torque wrench mode. (b) The extension DNA tether and angle of the cylinder is monitored in real time as the torsional stress in the DNA is relaxed. The force is held fixed at 0.5 pN.

Conclusion

In conclusion, we have presented a method for generating constant torque and monitoring a trapped particle's angular position within a single beam optical trap without the need to actively feedback on the torque signal. The passive torque wrench described here effectively reduces the angular trap stiffness to near zero, and thus the magnitude of the measured torque fluctuations are significantly reduced, and the torque provided by the trap can be much more precisely controlled. This trapping setup also allows for rapid switching between an angular trapping mode and a torque wrench mode without the need for additional beam paths or optics, reducing the possibility of systematic errors or crosstalk often found in multiple beam instruments. Such a device makes possible a number of interesting studies of biologically important systems, such as monitoring the rotational motion of a molecular motor as it works against a constant external torsional load, or measuring the relaxation kinetics of a mechanically torqued biomolecule.

Acknowledgements

The authors thank the members of the Wang laboratory for critical reading of the manuscript. This research was supported by GM059849 NIH grant and MCB-0820293 NSF grant to MDW, and a Molecular Biophysics Training Grant to Cornell. J. Inman and S. Forth have contributed equally to this work.

References

Bonin, K. D., Kourmanov, B. and Walker, T. G. (2002). "Light torque nanocontrol, nanomotors and nanorockers." Optics Express **10**(19): 984-989.

Bustamante, C., Bryant, Z. and Smith, S. B. (2003). "Ten years of tension: single-molecule DNA mechanics." Nature **421**(6921): 423-427.

Daniels, B. C., Forth, S., Sheinin, M. Y., Wang, M. D. and Sethna, J. P. (2009). "Discontinuities at the DNA supercoiling transition." Phys Rev E Stat Nonlin Soft Matter Phys **80**(4 Pt 1): 040901.

Deufel, C., Forth, S., Simmons, C. R., Dejgosha, S. and Wang, M. D. (2007). "Nanofabricated quartz cylinders for angular trapping: DNA supercoiling torque detection." Nature Methods **4**(3): 223-225.

Forth, S., Deufel, C., Sheinin, M. Y., Daniels, B., Sethna, J. P. and Wang, M. D. (2008). "Abrupt buckling transition observed during the plectoneme formation of individual DNA molecules." Physical Review Letters **100**(14): 148301.

Forth, S., Deufel, C., Sheinin, M. Y., Daniels, B., Sethna, J. P. and Wang, M. D. (2008). "Abrupt buckling transition observed during the plectoneme formation of individual DNA molecules." Phys Rev Lett **100**(14): 148301.

Friese, M. E. J., Nieminen, T. A., Heckenberg, N. R. and Rubinsztein-Dunlop, H. (1998). "Optical alignment and spinning of laser-trapped microscopic particles." Nature **394**(6691): 348-350.

Funk, M., Parkin, S. J., Stilgoe, A. B., Nieminen, T. A., Heckenberg, N. R. and Rubinsztein-Dunlop, H. (2009). "Constant power optical tweezers with controllable torque." Optics Letters **34**(2): 139-141.

Galajda, P. and Ormos, P. (2003). "Orientation of flat particles in optical tweezers by linearly polarized light." Optics Express **11**(5): 446-451.

La Porta, A. and Wang, M. D. (2004). "Optical torque wrench: Angular trapping, rotation, and torque detection of quartz microparticles." Physical Review Letters **92**(19): 190801.

McNaughton, B. H., Agayan, R. R., Clarke, R., Smith, R. G. and Kopelman, R. (2007). "Single bacterial cell detection with nonlinear rotational frequency shifts of driven magnetic microspheres." Applied Physics Letters **91**(22): 224105.

Paterson, L., MacDonald, M. P., Arlt, J., Sibbett, W., Bryant, P. E. and Dholakia, K. (2001). "Controlled rotation of optically trapped microscopic particles." Science **292**(5518): 912-914.

Sheinin, M. Y. and Wang, M. D. (2009). "Twist-stretch coupling and phase transition during DNA supercoiling." Physical Chemistry Chemical Physics **11**(24): 4800-4803.

Strogatz, S. H. (1994). Nonlinear Dynamics and Chaos. Reading, MA, Addison-Wesley.

Wang, M. D., Schnitzer, M. J., Yin, H., Landick, R., Gelles, J. and Block, S. M. (1998). "Force and velocity measured for single molecules of RNA polymerase." Science **282**(5390): 902-907.

Wood, T. A., Roberts, G. S., Eaimkhong, S. and Bartlett, P. (2008). "Characterization of microparticles with driven optical tweezers." Faraday Discussions **137**: 319-333.

CHAPTER 3

DNA Y STRUCTURE: A VERSATILE, MULTIDIMENSIONAL SINGLE MOLECULE ASSAY

Introduction

Optical trapping is a powerful single molecule technique used to study dynamic biomolecular events, especially those involving DNA and DNA-binding proteins. Current implementations usually involve only one of stretching, unzipping, or twisting DNA along one dimension. The study of more complex DNA-based systems requires a multi-dimensional technique that combines these manipulations in a single experiment. Here, we report a novel optical trapping assay based on a three-branch DNA construct, termed a "Y structure". This multi-dimensional assay allows precise, real-time tracking of multiple configurational changes. When the Y structure DNA is unzipped under both force and torque, the force and extension of all three branches can be determined simultaneously. The Y structure also provides a simple method to generate and study ssDNA. Moreover, the assay is readily compatible with fluorescence, as demonstrated by unzipping through a fluorescently labeled, paused transcription complex. This combination allowed both a detailed mapping of the RNA polymerase's interactions with DNA and visualization of its location before and after mechanical disruption.

Single molecule optical trapping techniques have enabled significant advancement in the understanding of a wide variety of biomolecular systems, especially those involving DNA and associated binding proteins. DNA-based systems have been manipulated and measured using three complementary implementations of optical trapping: stretching, unzipping, or twisting DNA. Stretching DNA with a bound

protein has yielded valuable information about dynamic protein-DNA interactions, such as nucleosome binding(Cui and Bustamante 2000; Bennink et al. 2001; Brower-Toland et al. 2002; Brower-Toland et al. 2005; Gemmen et al. 2005; Mihardja et al. 2006) and Rad51(van Mameren et al. 2009) or RecA(Forget and Kowalczykowski 2012) filament formation, and also allowed for tracking of DNA-based motor proteins such as RNA and DNA polymerases(Yin et al. 1995; Wang et al. 1998; Wuite et al. 2000; Smith et al. 2001; Adelman et al. 2004). A variation of the stretching method employing multiple traps has allowed bound proteins to be located(Dame et al. 2006; Noom et al. 2007). Unzipping DNA through a bound protein can provide detailed information about the strengths and locations of individual protein-DNA interactions(Koch et al. 2002; Koch and Wang 2003), and has been used to map the nucleosome structure at high resolution(Hall et al. 2009) and study nucleosome disruption by RNA polymerase(Jin et al. 2010). Unzipping DNA has also allowed helicase unwinding motion to be monitored(Dumont et al. 2006; Johnson et al. 2007; Sun et al. 2011). Twisting DNA has revealed that RNA polymerase can generate torques sufficient to melt DNA(Ma et al. 2013) and alter nucleosome structure(Sheinin et al. 2013).

While each of these techniques provides unique insights into biomolecular systems, they have only been combined in a limited fashion, with dynamic measurements made along one dimension. Complex biomolecular systems, such as transcription and replication machineries, involve processes that simultaneously stretch, unwind, and twist multiple strands of nucleic acids. Therefore the next generation of optical

trapping techniques will need to extend measurements to multiple dimensions to allow tracking of different configurational changes which occur simultaneously within molecular complexes.

New optical trapping assays should also be enhanced with fluorescence imaging to visualize molecular events on DNA. Previous studies have combined optical trapping with fluorescence(Ishijima et al. 1998; Lang et al. 2003; Dijk et al. 2004; Lang et al. 2004; Galletto et al. 2006; Hohng et al. 2007; Comstock et al. 2011; Heller et al. 2013), but force measurements were made along one dimension and fluorescence visualization of binding events was limited to a resolution of approximately a few hundred base pairs along long stretches of DNA. Future assays should extend fluorescence visualization of proteins to multi-dimensional DNA configurations, and could use fluorescence to establish a low resolution, 'big picture' map of protein locations while exploiting high-resolution optical trapping techniques to home in on their precise locations.

We present a novel multi-dimensional assay that allows simultaneous stretching, twisting, and unzipping of DNA. This assay, termed the "Y-structure", utilizes a dual-beam optical trap to hold a three-branch DNA construct. The forces and extensions of all three DNA branches are simultaneously measured, eliminating the constraint of a single axis of tension and allowing multiple configurational changes within a biomolecular system to be resolved independently. This assay also enables a simple way to generate and study ssDNA. The Y structure assay can be readily combined

with fluorescence to visualize binding events in all three DNA branches while DNA unzipping provides near base-pair resolution mapping of both the location of a bound complex and multiple, detailed interactions within a single complex. Thus this new technique provides a versatile, multi-dimensional platform for the study of complex biomolecular systems.

The Y structure

The Y structure is a three-way DNA junction which resembles a replication fork (**Fig. 1**). It is composed of three main branches: two DNA arms which are initially fully double stranded, and a dsDNA trunk. The end of the trunk is attached to a microscope coverslip, while the end of one arm is attached to a microsphere held in an optical trap (Trap 1), and the end of the other arm to a second microsphere held in a second, separate trap (Trap 2). Each microsphere can be manipulated separately by its trap and its three-dimensional (3D) force and position are detected. The coverslip is mounted onto an *x*-*y*-*z* piezo stage. This configuration allows for full 3D manipulation of the Y structure and measurements of force and extension in each branch.

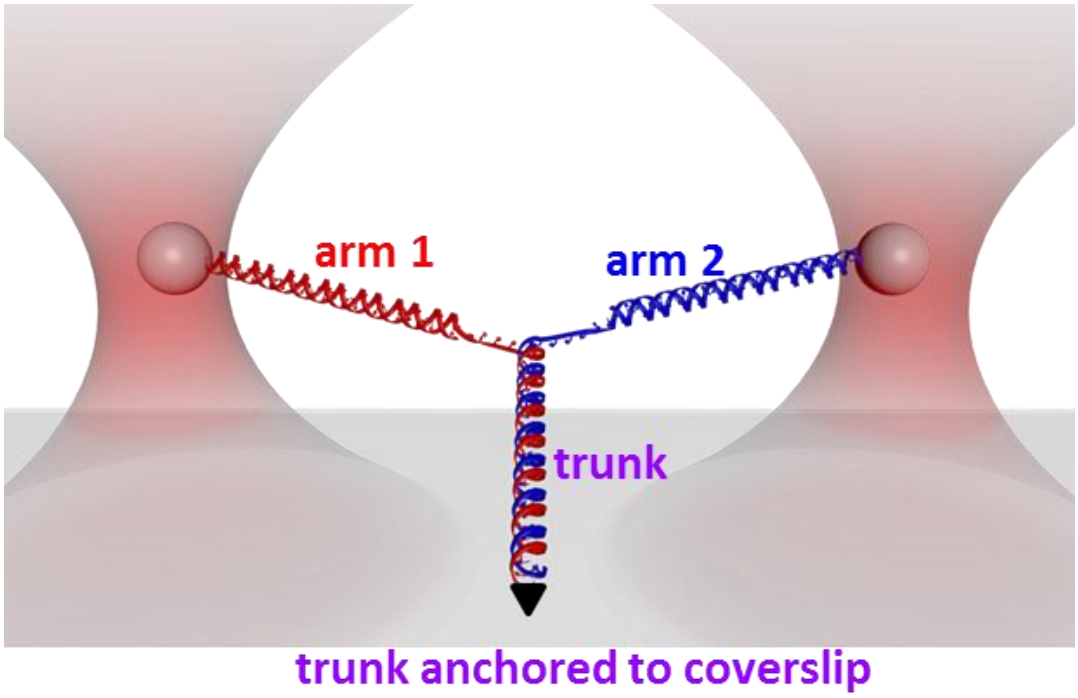

Figure 1. The Y structure experimental configuration. The initial Y structure consisted of two dsDNA arms which were joined to a dsDNA trunk: one arm was attached to an optically trapped microsphere via a streptavidin/biotin connection; the second arm to a second optically trapped microsphere via a digoxigenin/anti-digoxigenin connection; the trunk to a microscope coverslip via a fluorescein/anti-fluorescein connection. This version of the Y-structure contained a single anchoring point of the trunk via one of its two DNA strands and thus permitted the trunk end to swivel around the anchoring point without any torsional constraint.

Y structure construction

The Y structure DNA was constructed from three distinct dsDNA segments: two arms and the trunk (**Fig. 2**). The arms were made by restriction enzyme cuts from plasmid pMDW38 (sequence available upon request) for symmetric arms or from plasmid pRL574(Schafer et al. 1991) for asymmetric arms. A single restriction cut (XhoI or SphI) in this plasmid created an overhang that was subsequently filled in with either dig-dUTP or bio-dATP by Klenow polymerase (NEB) to provide specific attachment to anti-digoxigenin or streptavidin coated microspheres respectively. A second restriction cut (BstXI or BstEII) created an overhang for ligation to an annealed trunk adapter oligos to generate a long (>30 bp) overhang on each arm. The two trunk adaptor oligos from the two arms were complementary to each other and were subsequently annealed to form Y arms with a short trunk (~30 bp). The annealed adaptor oligos were designed to create an overhang for ligation to the full length trunk. Such a design is modular so that the trunk is interchangeable. Trunk DNA was made via PCR with a primer containing a 5' fluorescein for subsequent anchoring to an anti-fluorescein surface and then cut with a restriction enzyme (AlwNI) to provide the proper overhang for ligation to the Y arms.

The torsionally constrained trunk was made by ligation to a torsion adapter at the end of the Y trunk (sequence available upon request). The torsional adapter was ~500 bp made via PCR with a 1:5 mixture of dTTP:fluorescein-dUTP to provide multiple attachment points in both strands.

For the RNAP fluorescence experiments, an 'asymmetric' Y structure was made with two arms having different lengths in order to determine to which strand RNAP remained bound after unzipping. This was accomplished by cutting the arms out of the plasmid pRL574 with restriction enzymes to create a longer DNA (dig arm with SalI and BstEII; bio arm with SapI and BstXI). For the co-directional collision template, the trunk contained a T7A1 promoter with a transcription start site located at 1065 bp from the Y-junction. For the head-on collision template, the transcription start site was located at 1108 bp from the Y-junction.

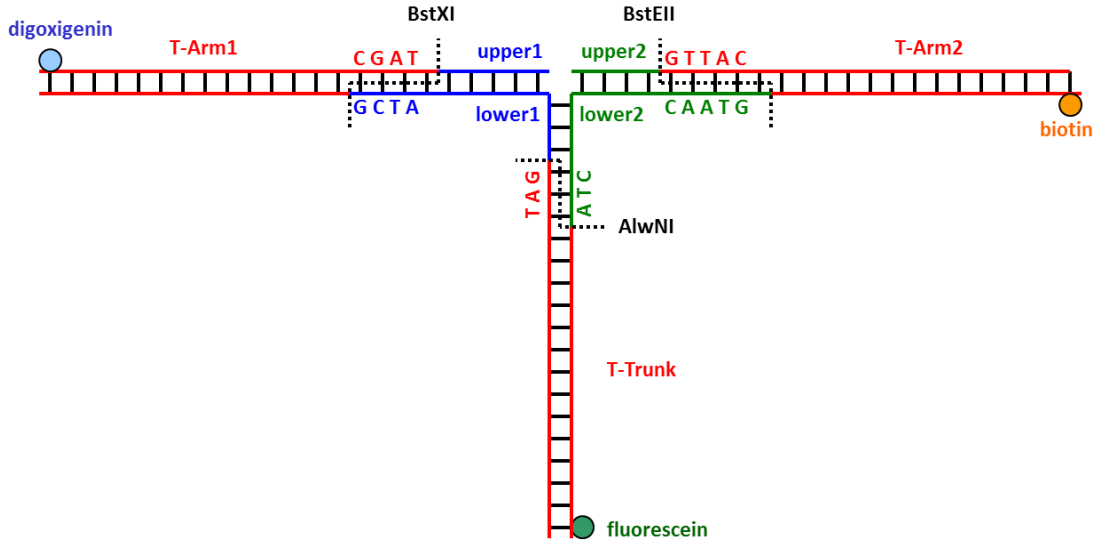

Figure 2. Construction of the Y structure. (1) Arm 1 DNA was cut from plasmid pMDW38 (sequence available upon request) and its 5' end was labeled with digoxigenin with a Klenow reaction. (2) Upper 1 (5'-/phos/GCA GTA CCG AGC TCA TCC AAT TCT ACA TGC CGC)and lower 1 (5'-/phos/GCC TTG CAC GTG ATT ACG AGA TAT CGA TGA TTG CG GCG GCA TGT AGA ATT GGA TGA GCT CGG TAC TGC ATC G) were annealed to form adapter 1. (3) Adapter 1 was ligated to arm 1 and the product was gel purified to remove un-ligated adapters. (4) Steps 1-3 were repeated for arm 2: upper 1 (5'-CGT TAC GTC ATT CTA TAC ACT GTA CAG) and lower 2 (5'-/phos/GTAAC CTG TAC AGT GTA TAG AAT GAC GTA ACG CGC AAT CAT CGA TAT CTC GTA ATC ACG TGC AAG GC CTA). (5) Arm 1 and arm 2 were annealed via lower 1 and lower 2. (6) Trunk DNA was prepared by PCR from pMDW2 (sequence available upon request) using a 5' fluorescein tag on one of the primers. (7) Arms were ligated to trunk DNA.

Instrument design

The dual optical trapping setup was a built upon a Nikon TE200 microscope with fluorescence and bright field microscopy capabilities (**Fig. 3**). The dual trap was created from a single laser source (Spectra Physics J20, 5 W) that was split into two beams by a polarizing beam splitting cube (PBSC) into orthogonal linear polarizations. One of the polarized beams was steered by a mirror mounted on a tip-tilt piezo (MCL Nano-MTA)(Moffitt et al. 2006). Although the two beams were orthogonally polarized, some interference between the two beams still existed due to the use of a high NA objective, leading to some cross talk between the two traps(Mangeol and Bockelmann 2008). To minimize this, we inserted optical windows in one of the two beams so that the path length difference between the beams was set to longer than the coherence length of the laser (3 mm). The two beams were recombined with another PBSC before entering a custom-built 'trapping port' which reflected the beams into the microscope objective with a dichroic mirror. The traps were formed at the focus of a water immersion objection (Nikon MRD07602). The two beams were collected by the condenser and split by a PBSC. Each polarized beam was detected by a quadrant photodiode (Pacific Silicon Sensor QP50-6SD2) by back focal-plane interferometry to provide positions and forces along *x* and *y* (lateral), and *z* (axial) directions for each microsphere in its trap. The flow cell was mounted on a 3D piezo stage (MCL Nano-LPQ) to allow movement of the coverglass surface relative to the traps.

Figure 3. A dual optical trap setup with bright field and fluorescence illumination. A 1064-nm Gaussian trapping beam is coupled to a polarization maintaining single mode fiber (not shown). After collimation, the beam is sent through a half-wave plate and beam splitter that controls the input power and ensures that the beam is linearly polarized. A second half-wave plate rotates the polarization and this partitions the power in the dual trap. The beam is re-collimated to ~ 5 mm by an expansion telescope and elevated to the proper height by a periscope. To form the dual trap, the single Gaussian laser beam is split into two orthogonally polarized beams by a polarizing beam splitting cube (PBSC) in the 'Beam Splitting Box'. One beam is reflected off of a mirror that is mounted on a tip/tilt piezo. This mirror is mapped to the back focal plane of the objective such that it controls Trap 1's position while Trap 2 remains fixed. The two beams are recombined by a second PBSC and expanded to ~ 10 mm by the mapping telescope. They are introduced into a Nikon TE200 microscope's imaging path and later to the trapping plane by a dichroic mirror. Upon exiting the condenser, the laser beams are reflected by a second dichroic mirror and again split by a PBSC. Each beam is detected by a quadrant photodiode (QPD). Bright field illumination is accomplished by 625-nm LED light introduced through the condenser lens. This light passes through the laser dichroic and the fluorescence cube set and is imaged by a cooled CCD. Fluorescence illumination is produced by a mercury arc lamp. The light is filtered and introduced into the illumination path by a fluorescence filter set optimized for quantum dots (excitation 350-450 nm, emission 625 nm).

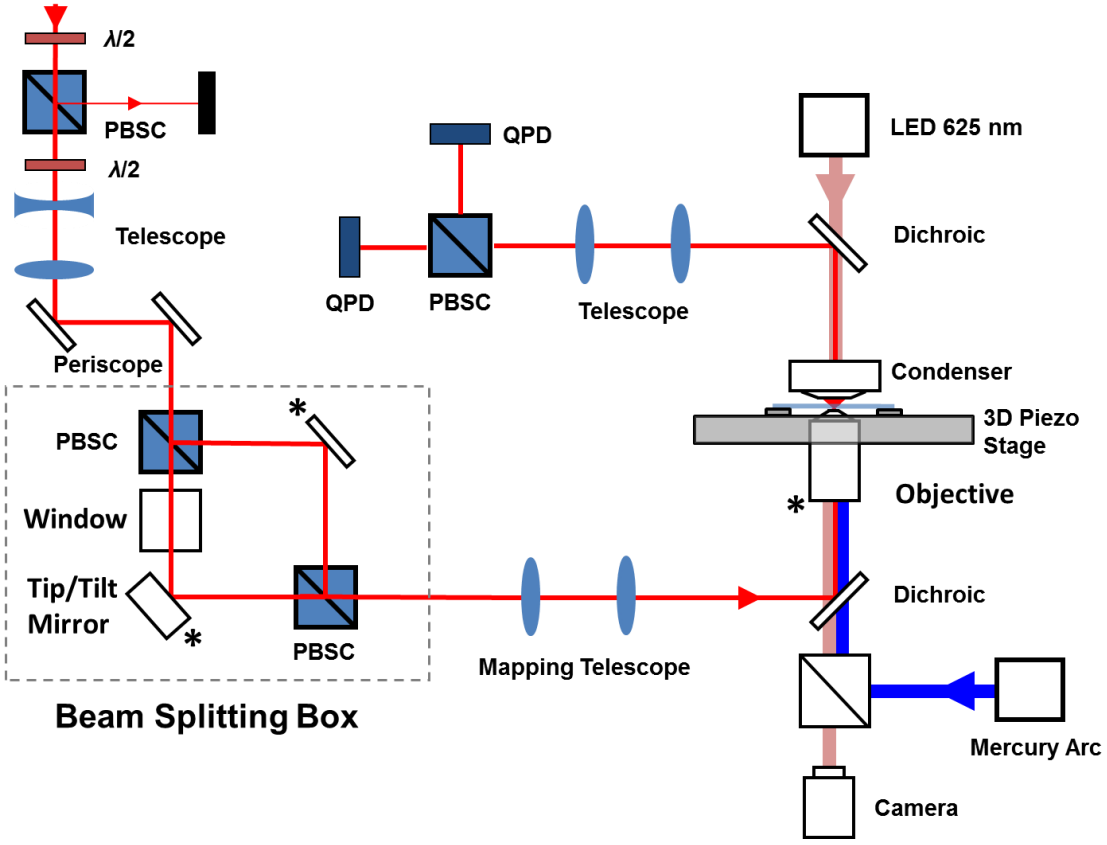
λ/2
PBSC
λ/2
Telescope
Periscope
PBSC
Window
Tip/Tilt
Mirror
PBSC
Beam Splitting Box
QPD
QPD
PBSC
Telescope
Mapping Telescope
LED 625 nm
Dichroic
Condenser
3D Piezo
Stage
Objective
Dichroic
Mercury Arc
Camera

Epi fluorescence was excited by a mercury arc lamp. The fluorescent cube set was designed for quantum dots with emission at 625 nm (Chroma 32214). Bright field illumination was accomplished with a red LED (625 nm, Thorlabs M625L2 and LEDD1B) which was transmitted by the 625 nm emission filter of the cube set. This allowed both the bright field and fluorescence images to be collected by the same cooled CCD (Hamamatsu ORCA-ER). To interlace the bright field and fluorescence images, the camera controller triggered the LED to turn on and off using a custom-built LED controller.

Data collection and analysis

During an experiment, Y-structures were identified as two microspheres in close proximity undergoing constrained Brownian motion. Custom software (LabVIEW 2010) was then used to automate several routines. First, prior to trapping a Y-structure, without microspheres in the trap, baseline data were recorded as the steered trap was scanned across the *xy* (lateral) plane. These baseline data were used to make corrections to experimental data. Second, the Y-structure anchoring point to the surface was centered between the two trapped microspheres by stretching the tether with the piezo stage using an algorithm similar to that previously described(Wang et al. 1997). Third, the height of the traps above the coverslip surface was determined by moving the coverslip towards the trapped microspheres and detecting the *z* piezo position when the microspheres came into contact with the surface(Deufel and Wang 2006). Fourth, the Y-structure was then stretched and unzipped by moving both the

steered trap and the piezo stage. A constant force on the trunk during unzipping experiments was maintained by feedback on the piezo stage. The laser power was also modulated to limit the displacement of a trapped microsphere from its trap center.

The 3D location for the junction of the Y-structure was determined as the intersection of the lines of force from the microspheres' positions. Thus the extensions of the three branches of the Y-structure were determined from the positions of the microspheres, the Y-structure anchoring point, and the Y-structure junction location. The forces on the arms were measured directly and the force on the trunk was determined by requiring the net force at the junction to be zero. Force and extension data for each arm were used for conversion to number of base pairs unzipped(Koch et al. 2002)

During an experiment, the 3D locations and force vectors of the two trapped microspheres as well as the position of the coverslip surface were measured in real time. To fully characterize the Y structure, the force and extension of each segment of the Y structure as well as the Y structure geometry were calculated from the raw data collected by our dual trap instrument. Below is a description of this calculation.

Below we refer to the coordinate system defined in **Fig. 4**. (1) The 3D location of the Y junction was determined. The *xy* location of the Y junction was located as the intersection of the lines of *xy* forces from the microspheres' positions (**Fig. 4a**). The *z* coordinate of the junction was determined by the geometry defined by the height of the microspheres above the surface and the *y* position of the junction (**Fig. 4b**). (2)

Once the position of the junction was known, the extension of each branch of the Y structure was determined as the distance between its two endpoints. (3) Finally, the force vectors on the arms were directly measured by the optical trap. The force on the trunk was determined by requiring that the net force at the junction to be zero (**Fig. 4c**). Thus, the force vector on the trunk was simply the opposite of the vector sum of the optical forces on the trapped microspheres.

The number of base pairs unzipped was calculated from the force and extension measurements described above. First, the force and extension of each branch of the Y structure were measured under lower forces (< 15 pN) prior to unzipping. These were taken as initial characterization of the Y structure. As the Y structure was unzipped, the extension in each arm at a given force increased beyond what could be accounted for by dsDNA alone. The additional extension was attributed to ssDNA. We used the modified freely-jointed-chain model of ssDNA(Smith et al. 1996; Wang et al. 1997) to calculate the number of base pairs of ssDNA in each arm. The ssDNA in the arms was a measure of the number of base pairs unzipped.

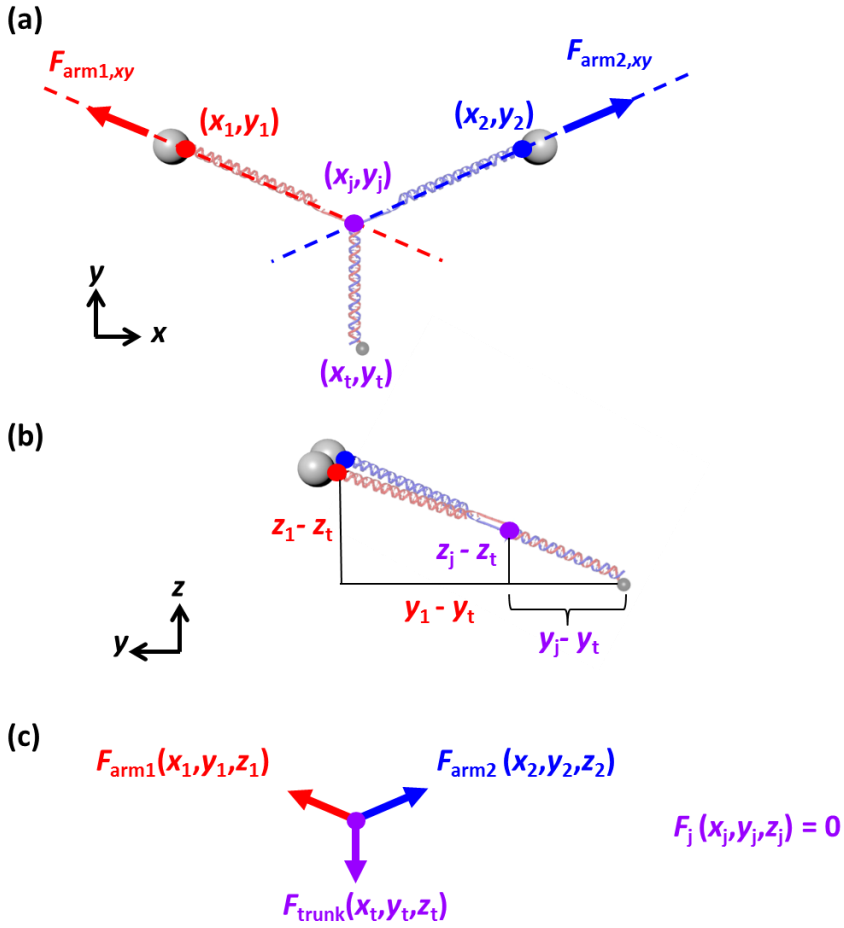

Figure 4. Calculation of Y structure forces and extensions.

(a) The projection of the Y structure onto the *xy* plane. The *xy* position of the Y junction is determined by the force and location of the trapped beads.

(b) The *z* location of the junction is determined by geometry.

(c) The forces are required to sum to zero at the junction.

To achieve near base pair resolution, the resulting force versus number of base pairs unzipped curve was aligned to the corresponding theoretical curve discussed in the next section using a cross-correlation method we previously developed(Shundrovsky et al. 2006; Hall et al. 2009; Li and Wang 2012) To account for minor instrumental drift, trapping-bead size variations, and DNA linker variations, the alignment allowed for a small additive shift (~ 20 bp) and a multiplicative linear stretch (~ 3%).

During fluorescence experiments, interlaced images of bright field and fluorescence were acquired by the CCD at 31.4 frames per second. To create an overlaid image a pair of bright field and fluorescence images were pseudo-colored and combined. To overlay the Y-structure configuration to indicate the three DNA segments, the 3D Y-structure configuration as determined from the optical trapping data was projected onto the *xy* plane and displayed as three white lines for the three DNA segments. The locations of the two microspheres were used as a reference to align the Y-structure to the images.

Unzipping under tension

Stretching DNA with a bound protein yields valuable information about protein-DNA interaction kinetics, while unzipping DNA provides detailed information about the locations and strengths of interactions. The Y structure makes it possible to combine DNA stretching and unzipping.

Here, we demonstrate DNA unzipping while maintaining a constant tension on the DNA trunk. Unzipping was achieved by two divergent forces, one from each arm, acting symmetrically about the trunk (**Fig. 5a**). The total force on the trunk was feedback controlled to maintain a constant value via modulation of Trap 1 and piezo stage positions. As Trap 1 was moved away from Trap 2, each of the two arms, which began as dsDNA, acquired ssDNA from the trunk as the trunk was unzipped, similar to 1D unzipping(Bockelmann et al. 1997) except that the DNA trunk was under tension.

Fig. 5b is an example of data acquired during the symmetric unzipping of a Y structure. As the Y structure was mechanically unzipped, the magnitudes of forces on both arms varied in an essentially identical fashion with the progression of unzipping, while the force on the trunk remained at the set point of 10 pN. The trunk extension decreased with time with concurrent extension increases in both arms. The angles between the arms and the trunk also varied with the progression of unzipping in an essentially identical fashion, further indicating that forces from the two arms were kept nearly symmetric.

Figure 5. Measurements of forces and extension while unzipping the Y structure

(**a**) Y structure geometry and force balance. The trunk dsDNA was mechanically unzipped by pulling on the arms with the two optical traps. The force vector on each arm was independently measured and thus the force on the trunk was determined by force balance at the junction. The 3D position of each trapped microsphere and the trunk anchoring point were also measured.

(**b**) An example data trace from symmetric unzipping of the trunk of a Y structure under a constant force on the trunk. The force and extension of each branch of the Y-structure as well as the angles of the Y-structure were measured as functions of time.

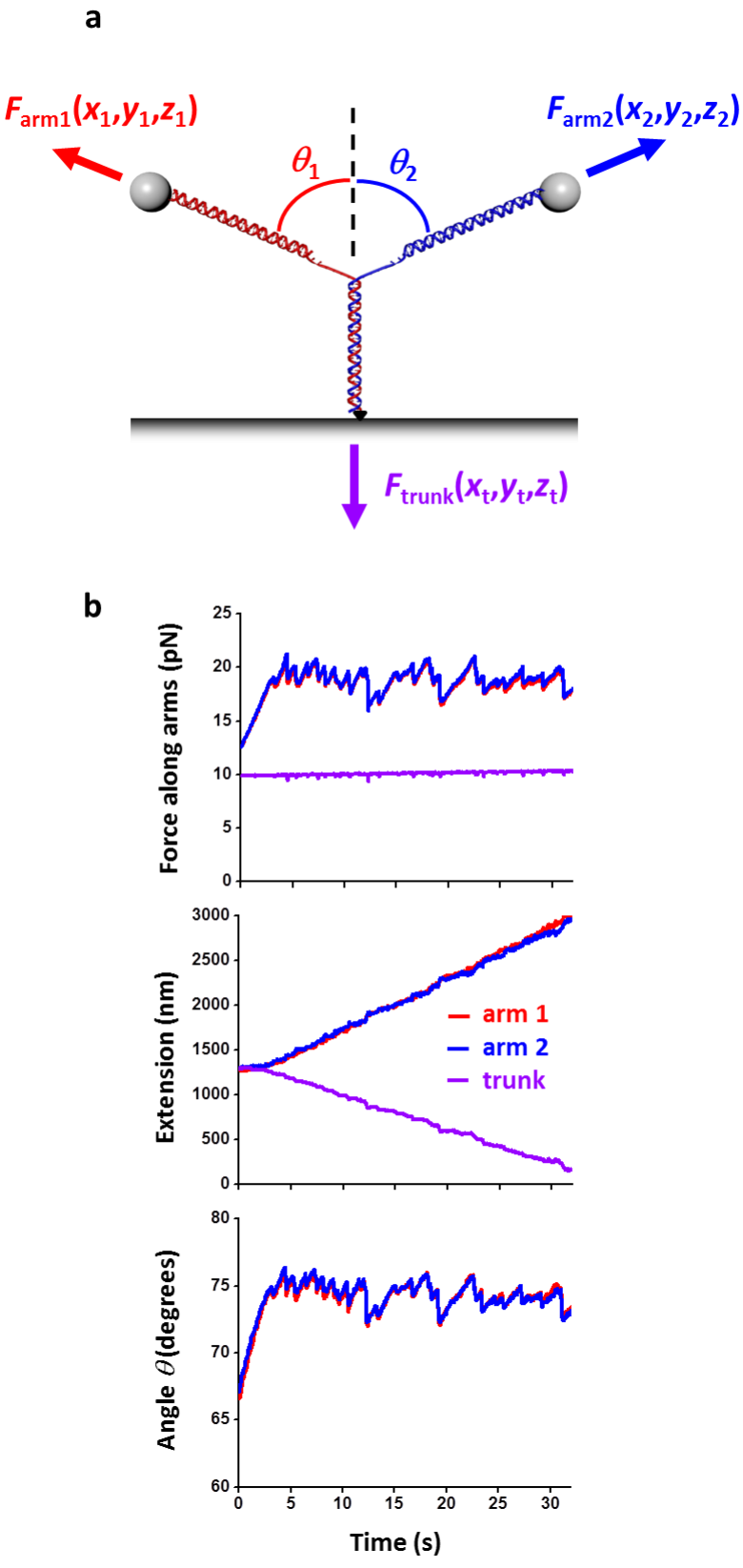
a
$F_{arm1}(x_1,y_1,z_1)$
$F_{arm2}(x_2,y_2,z_2)$
θ_1
θ_2
$F_{trunk}(x_t,y_t,z_t)$
b
Force along arms (pN)
Extension (nm)
arm 1
arm 2
trunk
Angle θ(degrees)
Time (s)

In order to understand these mechanical measurements, we extended a previous statistical mechanical model for 1D unzipping(Bockelmann et al. 1998) to the 2D unzipping configuration of the Y-structure (**see Theoretical models of Y structure unzipping**). This generalization takes into account the total free energy of the Y structure: the sequence-dependent DNA base pairing energy in the trunk dsDNA(Huguet et al. 2010), and the elastic free energies in both arms and trunk(Marko and Siggia 1995; Smith et al. 1996; Wang et al. 1997). The resulting partition function allows the calculation of the equilibrium forces in both arms and the equilibrium fork junction position.

The measured force along the arms versus number of base pairs unzipped agrees well with theory (**Fig. 6a**). This theory indicates that the force variation is solely a result of DNA sequence variations in the trunk, as would also be the case for 1D unzipping. Both measurements and theory show that the unzipping force profile, when the trunk is under tension, is similar to that when the trunk is under no tension, except for an overall increase in force.

To better characterize this force increase, we determined the force in the arms as a function of the force in the trunk (**Fig. 6b**). The force in the arms increased rather linearly with the force in the trunk. Even the force component perpendicular to the trunk is greater than that of the corresponding 1D unzipping force under the conditions we explored (**Fig. 6c,d**). The increased force indicates that the trunk of the Y structure is less destabilized than in the 1D unzipping case.

Figure 6. Unzipping a Y structure under different trunk forces.

(**a**) Force along arms versus number of base pairs unzipped under no trunk force (black) and 10 pN trunk force (red). Since the measured forces along the two arms were nearly identical, their mean force was used to make these plots. Theoretical predictions are shown for comparison.

(**b**) Mean force along arms versus force along trunk (black). For each trunk force, force along arms was averaged over the first 1500 bp unzipped. Theoretical prediction is shown in red.

(**c**) Component of force along arms perpendicular to the trunk versus number of base pairs unzipped under no trunk force (black) and 10 pN trunk force (red). Theoretical predictions are shown for comparison.

(**d**) Component of mean force along arms perpendicular to the trunk versus force along trunk (black). For each trunk force, component of the force along arms perpendicular to the trunk was averaged over the first 1500 bp unzipped. Theoretical prediction is shown in red.

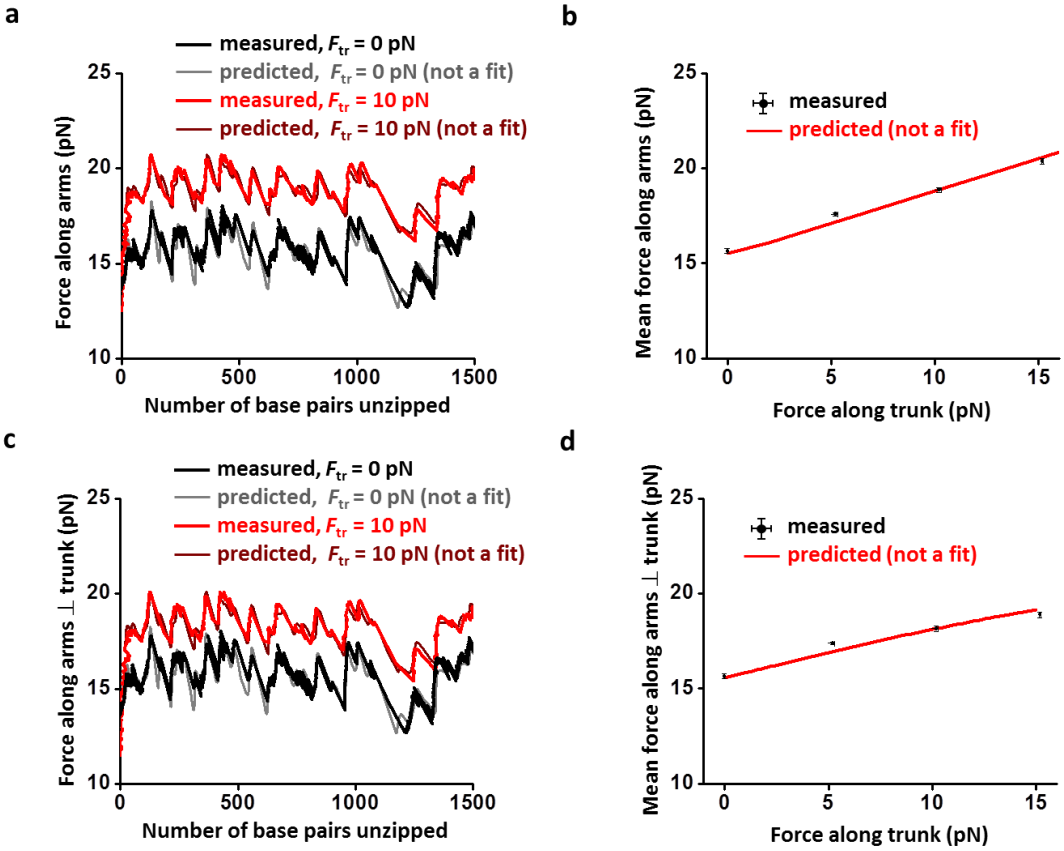
a
measured, F_{tr} = 0 pN
predicted, F_{tr} = 0 pN (not a fit)
measured, F_{tr} = 10 pN
predicted, F_{tr} = 10 pN (not a fit)
Force along arms (pN)
Number of base pairs unzipped
b
measured
predicted (not a fit)
Mean force along arms (pN)
Force along trunk (pN)
c
measured, F_{tr} = 0 pN
predicted, F_{tr} = 0 pN (not a fit)
measured, F_{tr} = 10 pN
predicted, F_{tr} = 10 pN (not a fit)
Force along arms ⊥ trunk (pN)
Number of base pairs unzipped
d
measured
predicted (not a fit)
Mean force along arms ⊥ trunk (pN)
Force along trunk (pN)

Generation and manipulation of long ssDNA

ssDNA is an important substrate, or intermediate, during replication, DNA repair and recombination, where long stretches of thousands of base pairs of ssDNA are operated on by a variety of proteins. It has been experimentally challenging to generate and manipulate long ssDNA of arbitrary sequence using an optical trap. Previous methods relying on DNA stretching require the application of high force (~ 65 pN) and/or chemical reagents(Smith et al. 1996; Hegner et al. 1999; Candelli et al. 2013) or the use of enzymatic reactions(Ibarra et al. 2009) to facilitate strand separation. Methods using DNA unzipping do not subject a DNA molecule to excessive forces but yield ssDNA of complementary sequences that anneal upon force reduction(Bockelmann et al. 1997; Koch et al. 2002).

Here, we demonstrate the use of the Y structure, first to generate ssDNA of many kilo-base pairs of arbitrary sequence, and then to manipulate it from low to high forces. In order to generate ssDNA, we used a Y-structure version with only one strand of its trunk end attached to the microscope coverslip (**Fig. 5a**). The dsDNA trunk was then unzipped to completion using a method similar to that described in **Fig. 5** and **Fig. 6**. Once the trunk was fully unzipped, one strand of the trunk remained attached to the coverslip and was composed of one dsDNA arm and the ssDNA of the trunk of the original Y structure (**Fig. 7a**). The other strand, and its associated arm, retracted to their trapped microsphere which was subsequently released into solution. The remaining tether was then stretched with one of the traps and its force-extension curve

was measured. After removing the contribution to the force-extension from the dsDNA arm(Wang et al. 1997), the force-extension curve of the ssDNA was obtained (**Fig. 7b**). The force-extension of ssDNA was well characterized by a modified freely-jointed chain model(Smith et al. 1996) at forces > 10 pN, yielding fit parameters in good agreement with those previously established(Smith et al. 1996; Koch et al. 2002). Below this force, the relation showed less well defined features, as a result of the formation of secondary structures in the ssDNA at low forces(Dessinges et al. 2002; Johnson et al. 2007).

Figure 7. Generating and stretching long ssDNA tethers.

(**a**) Cartoons depicting the steps to generate a long ssDNA tether. The initial Y structure contained a trunk with only one strand of the trunk end attached to the coverslip surface. The Y structure was then fully unzipped to release the other trunk strand from the surface. The remaining tether was composed of a dsDNA segment that had been one of the original arms and a newly generated long stretch of ssDNA that had been part of the original trunk dsDNA. This tether was subsequently stretched to obtain a force-extension curve of the composite dsDNA and ssDNA.

(**b**) Force versus extension of ssDNA. The force-extension curve of the ssDNA was obtained after removing the contribution of the dsDNA from the measured force-extension of the composite DNA. The resulting ssDNA force-extension (black) was fit to a modified freely-jointed chain model (solid red) at forces > 10 pN, yielding a persistence length of 0.765 nm, a stretch modulus of 470 pN, and a contour length of 2055 nm. Below 10 pN, an extrapolation of the fit is shown.

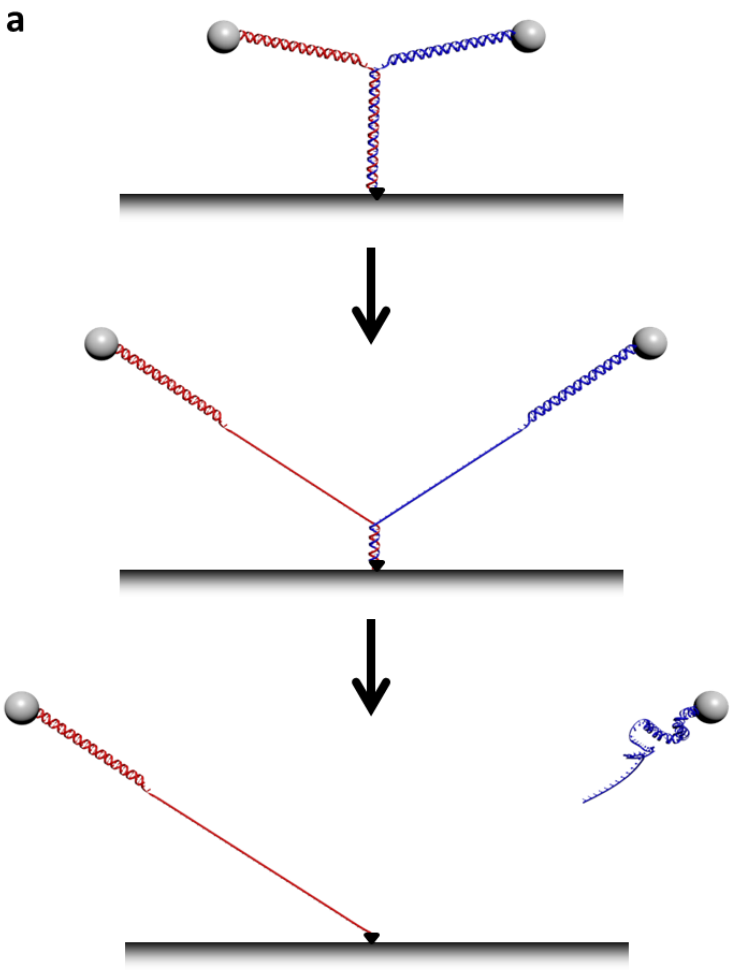
a

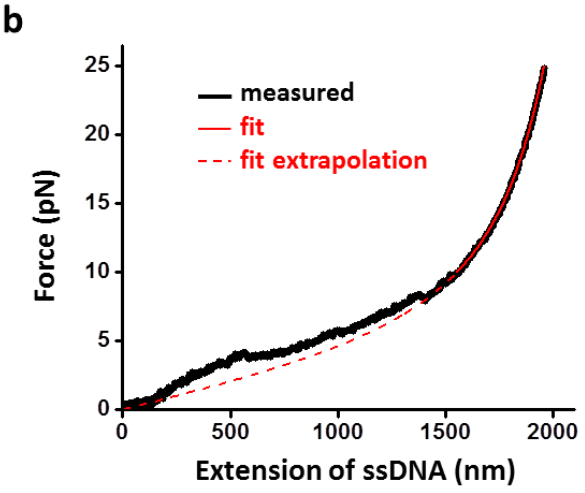
b
measured
fit
fit extrapolation
Force (pN)
0
5
10
15
20
25
0
500
1000
1500
2000
Extension of ssDNA (nm)

Torsion generation

Due to the helical nature of dsDNA, motor proteins that translocate along DNA will necessarily have to rotate relative to the DNA. Hindrance of relative rotation by cellular constraints and viscous drag leads to torsion build-up that in turn regulates these processes(Koster et al. 2010; Forth et al. 2013). Thus torsion in DNA plays an important role in biological processes that take place on DNA and has been demonstrated to significantly alter activities of bound proteins(Ma et al. 2013). The Y structure provides a natural way to create and control torsion in the trunk DNA.

In order to demonstrate this feature, we torsionally anchored the end of the trunk to the surface of a coverslip via multiple attachment points (Methods) (**Fig. 8a**). This enabled the introduction of twist to the trunk DNA by unzipping the DNA. During the unzipping of the Y structure, the fork end of the trunk is expected to rotate, converting twist released from base pairing to additional twist in the trunk. This buildup in twist energy should make it progressively more difficult to unzip the trunk.

Fig. 8b shows measurements from unzipping a torsionally constrained trunk which was held under 4 pN of tension, sufficient force to prevent buckling of the trunk DNA in our experiment. As expected, unzipping force indeed increased rapidly, even upon a small amount of unzipping. The force increase was linear, with respect to the number of base pairs unzipped, and was modulated by variations due to DNA

sequence. In comparison, when the trunk was not under torsion, the unzipping force remained essentially constant, aside from the sequence-dependent variations.

To better understand these measurements, we further extended the theoretical model to consider the unzipping of the Y structure under torsion in addition to tension (**Fig. 8b**, **Theoretical models of Y structure unzipping**). The theory correctly predicts the force increase and the sequence-dependent force variations. It also provides a simple explanation for the linearity in the force increase, which results from the torsional energy's quadratic dependence on the twist of the trunk(Marko 2007).

Even without DNA unzipping, the Y structure provides a flexible way of generating twist in the trunk. For example, twist may be added to the trunk DNA by rotation of the two dsDNA arms about the trunk attachment point.

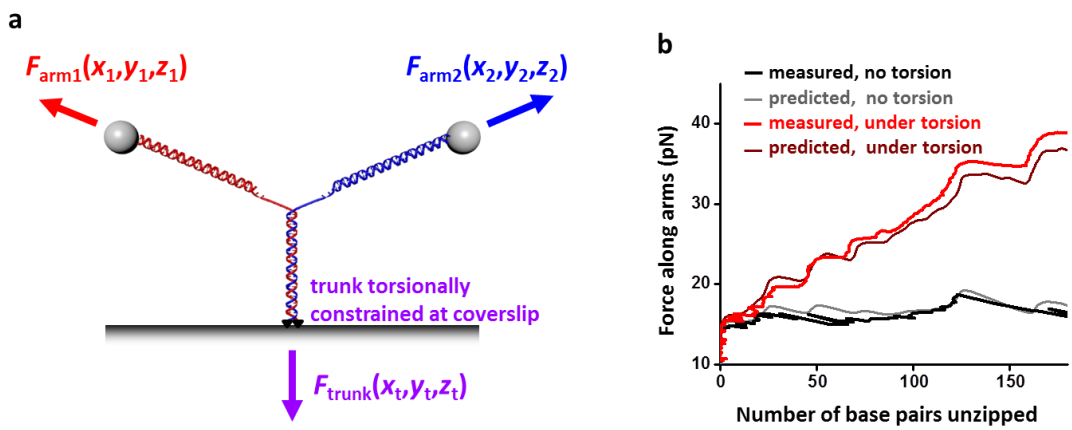

Figure 8. Unzipping a Y structure under torsion.

(**a**) The trunk of the Y structure was torsionally constrained to the microscope coverslip via multiple fluorescein/anti-fluorescein connections at both DNA strands of the trunk end. This Y structure version prevented the trunk end from swiveling around the anchoring points.

(**b**) Force along arms versus number of base pairs unzipped of either a torsionally constrained or unconstrained trunk, both under 8 pN trunk force. Theoretical predictions are shown for comparison.

Theoretical models of Y structure unzipping

We have extended a previous theoretical model of 1D DNA unzipping using equilibrium statistical mechanics methods(Bockelmann et al. 1997; Bockelmann et al. 2002; Huguet et al. 2010; Gross et al. 2011) to model 2D DNA unzipping of a Y structure.

For this section, to simplify notation, we consider a symmetric Y structure initially consisting of two arms, each of n_{arm} base pairs of dsDNA, and a trunk of n_{tr} base pairs of dsDNA (**Fig.9**). As the trunk is unzipped by n base pairs, n nucleotides of ssDNA are added to each arm while the trunk reduces to $(n_{\mathrm{tr}} - n)$ base pairs of dsDNA. For simplicity, we assume that the trunk is unzipped by two arm forces symmetric about the trunk, and the Y structure lies in the xz plane with the trunk end at $(0,0)$, arm 1 end at $(-x_{\mathrm{a}}, z_{\mathrm{a}})$, and arm 2 end at $(+x_{\mathrm{a}}, z_{\mathrm{a}})$. The junction location and forces in each branch are determined by requiring the net force at the junction to be zero, using the measured force-extension relations.

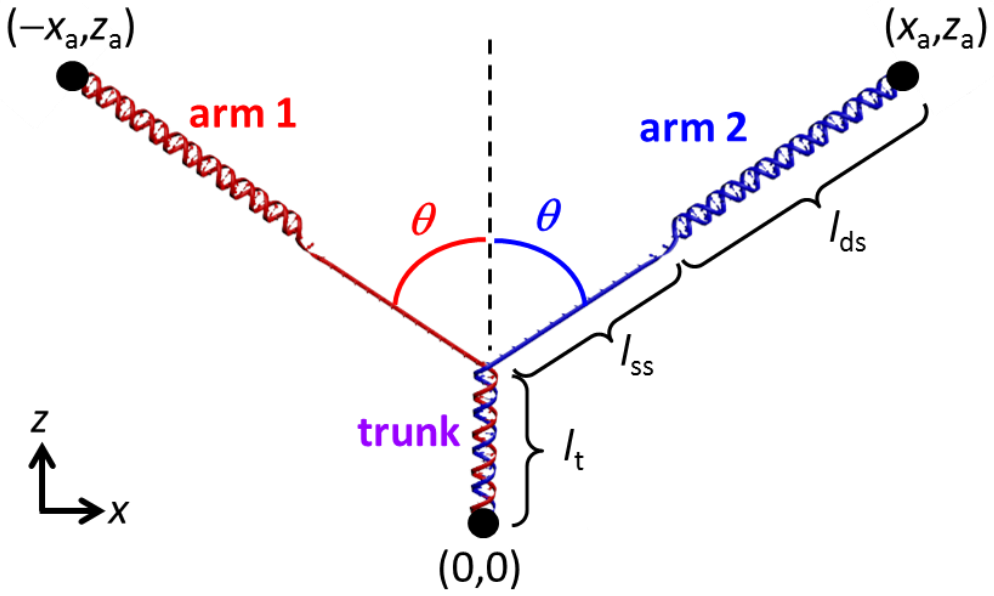

Figure 9. Geometry of the Y structure for theoretical modeling. The Y structure is confined to the *xz* plane and is symmetric about the trunk. The extension of each segment of DNA is indicated: l_t for the dsDNA trunk, l_{ss} for ssDNA in each arm, and l_{ds} for dsDNA in each arm.

The force-extension relation per nucleotide of ssDNA(Smith et al. 1996) is:

$$\frac{s_{\mathrm{ss}}}{L_{0\_\mathrm{ss}}} = \left[\coth\left(\frac{2f_{\mathrm{ss}}L_{\mathrm{p\_ss}}}{k_{\mathrm{B}}T}\right) - \frac{k_{\mathrm{B}}T}{2f_{\mathrm{ss}}L_{\mathrm{p\_ss}}}\right]\left(1 + \frac{f_{\mathrm{ss}}}{K_{0\_\mathrm{ss}}}\right), \quad (1)$$

where f_{ss} is the force, s_{ss} the extension per nucleotide, L_{0_ss} the contour length per nucleotide of ssDNA, $L_{\mathrm{p\_ss}}$ the persistence length of ssDNA, K_{0_ss} the stretch modulus of ssDNA, and $k_{\mathrm{B}}T$ the thermal energy. Using the Y structure as described in the main text (**Fig. 3b**), we measured L_{0_ss}, $L_{\mathrm{p\_ss}}$, K_{0_ss}, and $k_{\mathrm{B}}T$ to be 0.55 nm, 0.79 nm, 470 pN, and 4.11 pN·nm respectively under our experimental conditions (**Fig. 10**).

The force-extension per base pair of dsDNA(Wang et al. 1997) is:

$$f_{\mathrm{ds}} = \frac{k_{\mathrm{B}}T}{L_{\mathrm{p\_ds}}}\left[\frac{1}{4\left(1 - s_{\mathrm{ds}}/L_{0\_\mathrm{ds}} + f_{\mathrm{ds}}/K_{0\_\mathrm{ds}}\right)} - \frac{1}{4} + \frac{s_{\mathrm{ds}}}{L_{0\_\mathrm{ds}}} - \frac{f_{\mathrm{ds}}}{K_{0\_\mathrm{ds}}}\right], \quad (2)$$

where f_{ds} is the force, s the extension per base pair, L_{0_ds} the contour length per base pair of dsDNA, $L_{\mathrm{p\_ds}}$ the persistence length of dsDNA, and K_{0_ds} the stretch modulus of dsDNA. We used previously measured values of L_{0_ds}, $L_{\mathrm{p\_ds}}$, and K_{0_ds} of 0.34 nm, 43 nm, and 1200 pN respectively(Wang et al. 1997) (**Fig. 10**).

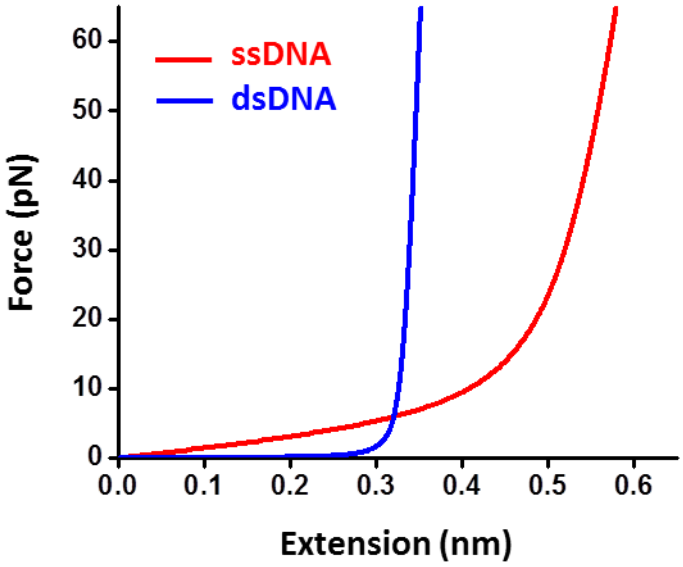

Figure 10. Force-extension curves of ssDNA and dsDNA. Shown are extensions per nucleotide of ssDNA (red) and per base pair of dsDNA (blue) as determined by measured DNA elasticity parameters. See Eqs. (1) and (2).

Once x_a, z_a, and n are specified and the ssDNA and dsDNA elastic properties are determined, the junction location is determined based on force balance, yielding the trunk extension l_t, ssDNA extension in each arm l_{ss}, and dsDNA extension in each arm l_{ds}, as well as forces in each branch (**Fig. 9**). Thus the state of the Y structure is fully defined by the positions of the three end points of the Y structure and the number of base pairs unzipped, i.e., x_a, z_a, and n. Below we consider unzipping under four different scenarios.

The Y structure under constant end positions

Consider a scenario where the trunk DNA of the Y structure is unzipped such that the ends of the arms are at specified positions (i.e., x_a and z_a are given and held fixed). Under thermal agitation, the fork junction may still fluctuate over multiple states, each with a different number of base pairs (n) unzipped. We wish to find the equilibrium fork junction position and the equilibrium forces in the three branches. Our general strategy is to determine the free energies at all possible states, use these energies to define the partition function of the system, and then use the partition function to determine the equilibrium value (mean value) of any parameter of interest.

The free energy of the Y structure at a given state consists of two distinct components:

$$G(n; x_a, z_a) = G_{DNA}(n) + G_{stretch}(n; x_a, z_a) \ . \tag{3}$$

The first term $G_{DNA}(n)$ is free energy increase due to the loss of base pairing of the first n base pairs unzipped, and can be determined using the nearest-neighbor model with corrections that take into account the temperature and salt conditions used in the experiments(Huguet et al. 2010). The second term $G_{\mathrm{stretch}}(n; x_{\mathrm{a}}, z_{\mathrm{a}})$ is the work to stretch each branch of the Y structure to the specified state:

$$G_{\mathrm{stretch}}(n; x_{\mathrm{a}}, z_{\mathrm{a}}) = 2G_{\mathrm{ds,arm}}(n_{\mathrm{arm}}, l_{\mathrm{ds}}) + 2G_{\mathrm{ss,arm}}(n, l_{\mathrm{ss}}) + G_{\mathrm{ds,trunk}}(n_{\mathrm{tr}} - n, l_{\mathrm{t}}) \,, \tag{4}$$

For ssDNA of n nucleotides to stretch to extension l (**Fig. 11**), the free energy is

$$G_{\mathrm{ss}}(n, l) = n \int_0^{l/n} f_{\mathrm{ss}}(s_{\mathrm{ss}}) ds_{\mathrm{ss}} \,. \tag{5}$$

For dsDNA of n base pairs to stretch to extension l (**Fig. 11**), the free energy is

$$G_{\mathrm{ds}}(n, l) = n \int_0^{l/n} f_{\mathrm{ds}}(s_{\mathrm{ds}}) ds_{\mathrm{ds}}. \tag{6}$$

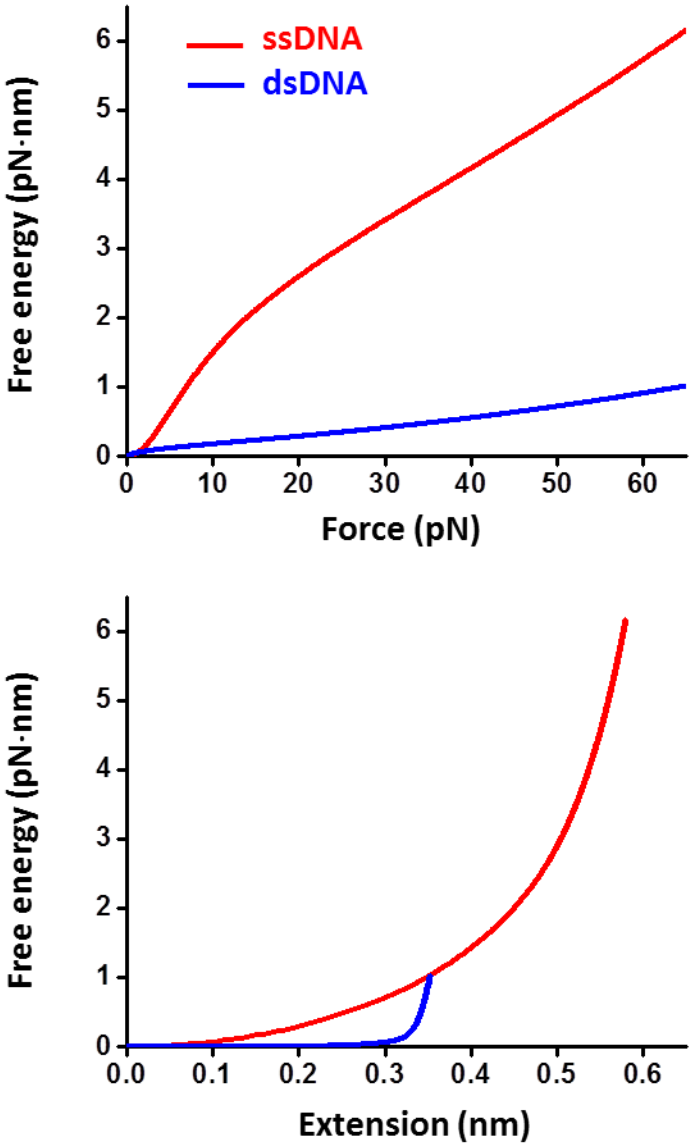

Figure 11. Energies to stretch ssDNA and dsDNA. Shown are the energies needed to stretch one nucleotide of ssDNA (red) and one base pair of dsDNA (blue) to specified extension and force.

Given x_{a} and z_{a}, we numerically calculate the extensions of all DNA segments for each possible value of n using the "fsolve" routine of the SciPy package of Python. The results of this calculation are then used to calculate $G(n; x_{\mathrm{a}}, z_{\mathrm{a}})$, which yields the partition function. The average number of base pairs unzipped $\langle n \rangle$ and the average force $\langle F_i \rangle$ (i = 1 to 3, one for each branch) are determined from the partition function:

$$\langle n \rangle = \frac{\sum_n n \, exp(-G(n;x_{\mathrm{a}},z_{\mathrm{a}})/k_{\mathrm{B}}T)}{\sum_n exp(-G(n;x_{\mathrm{a}},z_{\mathrm{a}})/k_{\mathrm{B}}T)} \tag{7}$$

$$\langle \vec{F_i} \rangle = \frac{\sum_n \vec{F_i} \, exp(-G(n;x_{\mathrm{a}},z_{\mathrm{a}})/k_{\mathrm{B}}T)}{\sum_n exp(-G(n;x_{\mathrm{a}},z_{\mathrm{a}})/k_{\mathrm{B}}T)} \tag{8}$$

Fig. 12 shows some results of these calculations. At a small value of $(z_{\mathrm{a}} - l_{\mathrm{t}})$, the mean unzipping force along arms is comparable to the corresponding 1D unzipping force which fluctuates around ~ 15 pN. The force along arms and the trunk force increase with a more extended Y structure in z and/or more base pairs unzipped.

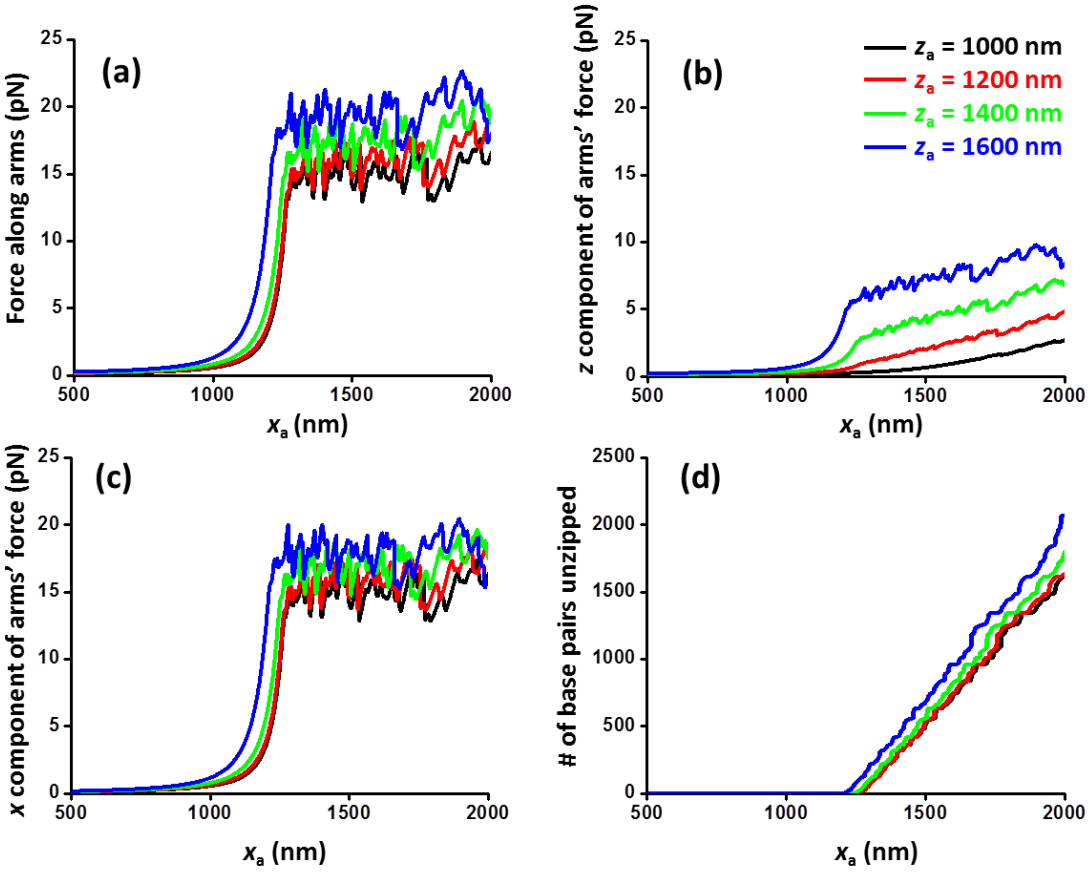

Figure 12. Forces under constant end positions of the Y structure. Results are shown for several values of z_a positions.

(a) Force along arms versus x_a.

(b) z component of arms' mean force versus x_a.

(c) x component of arms' mean force versus x_a.

(d) Number (#) of base pairs unzipped versus x_a.

The Y structure under constant trunk force

Next we consider a scenario where the trunk DNA of the Y structure is unzipped under a constant trunk force ($F_{\mathrm{tr}} = 2F_{\mathrm{a},z}$) such that the x coordinates of the ends of the arms are specified (i.e., F_{tr} and x_{a} are given and held fixed). To calculate arm force in this situation, the free energy must be a function of x_{a} and F_{tr} instead of x_{a} and z_{a}. We refer to this free energy as $G_1(n; x_{\mathrm{a}}, F_{\mathrm{tr}})$ which relates to $G(n; x_{\mathrm{a}}, z_{\mathrm{a}})$ via the Legendre transform by subtracting the product of the conjugate variables z_{a} and F_{tr}:

$$G_1(n; x_{\mathrm{a}}, F_{\mathrm{tr}}) = G(n; x_{\mathrm{a}}, z_{\mathrm{a}}) - z_{\mathrm{a}}F_{\mathrm{tr}}. \tag{9}$$

Since

$$\frac{\partial G(n; x_{\mathrm{a}}, z_{\mathrm{a}})}{\partial y_{\mathrm{a}}} = F_{\mathrm{tr}}, \tag{10}$$

Eq. (10) allows Eq. (9) to be expressed solely in terms of n, x_{a}, and F_{tr}. Eq. (9) indicates that the free energy $G_1(n; x_{\mathrm{a}}, F_{\mathrm{tr}})$ lowers with an increase in the trunk force.

Once $G_1(n; x_{\mathrm{a}}, F_{\mathrm{tr}})$ is determined, the arm force and the number of base pairs unzipped can be found using a partition function of the form in Eqs. (7) and (8) by replacing $G(n; x_{\mathrm{a}}, z_{\mathrm{a}})$ with $G_1(n; x_{\mathrm{a}}, F_{\mathrm{tr}})$. **Fig. 13** shows some results of these calculations. As with the scenario where the ends of the Y structure are held at fixed positions, this scenario also shows that at low trunk force, the arm force is comparable to the 1D unzipping force. As the trunk force increases, the arm force also increases.

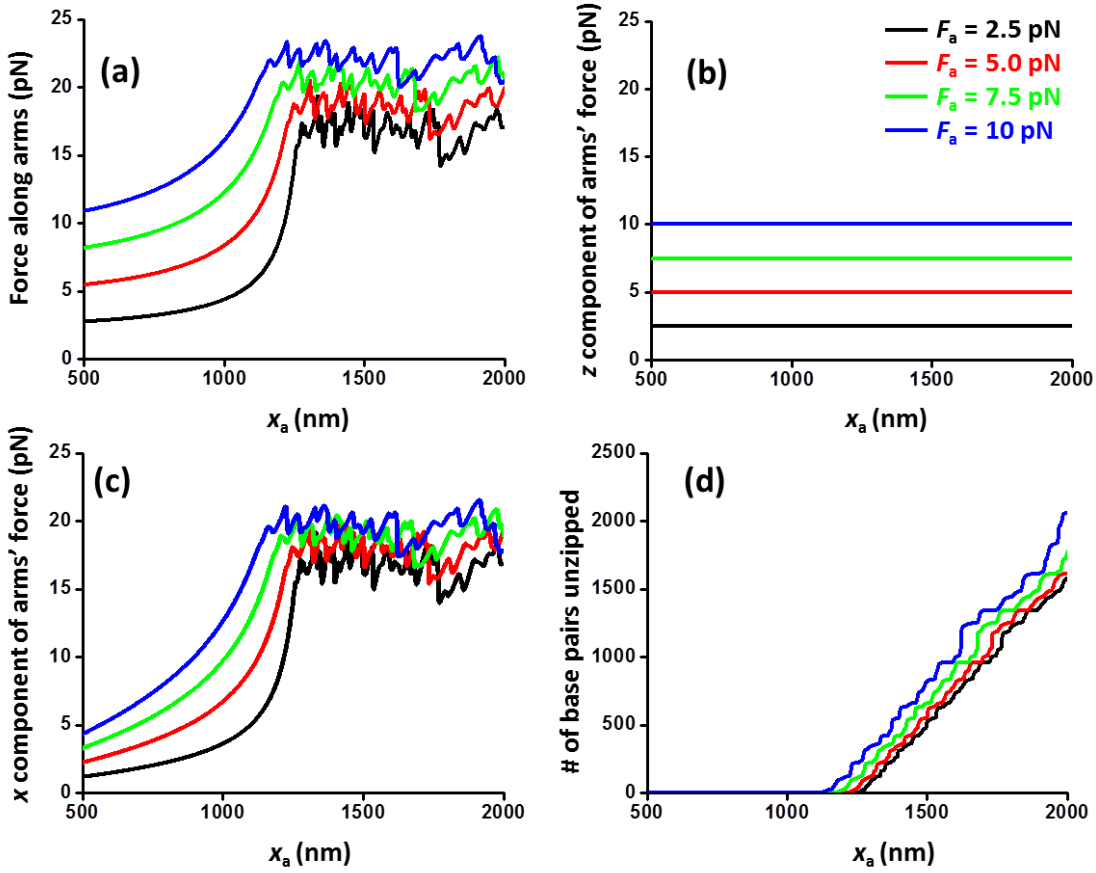

Figure 13. Arm forces under a constant trunk force of the Y structure. Results are shown for several values of the trunk forces.

(a) Force along arms versus x_a.

(b) z component of arms' mean force versus x_a.

(c) x component of arms' mean force versus x_a.

(d) Number (#) of base pairs unzipped versus x_a.

The Y structure under torsional constraint

We now consider a scenario where the trunk end is torsionally constrained and the trunk DNA is unzipped under a constant trunk force ($F_{\mathrm{tr}} = 2F_{\mathrm{a},z}$) such that the x coordinates of the ends of the arms are specified (i.e., F_{tr} and x_{a} are given and held fixed). As the trunk DNA is unzipped, the linking number in the trunk remains constant while the trunk shortens, resulting in overtwisting of the trunk. Continued torque buildup will eventually lead to a phase transition to plectonemic DNA or P-DNA(Deufel et al. 2007; Forth et al. 2008; Daniels et al. 2009; Sheinin and Wang 2009; Forth et al. 2013). We will limit our discussion to consider only the B-DNA regime prior to any phase transition.

To calculate the arm force, the free energy outlined in the previous section needs to be modified to take into account the torsional energy in the trunk. Torsional energy may be expressed in terms of the degree of supercoiling, σ, defined as the number of turns introduced into the DNA per natural number of turns in the DNA. Under moderate forces and small degrees of supercoiling, the twist energy depends on σ quadratically and is also a function of the force (F) in the DNA(Marko 2007; Sheinin and Wang 2009):

$$G_{\mathrm{twist}}(F, \sigma, L_0) = +\frac{L_0 c_s}{2}\sigma^2, \tag{11}$$

with

$$c_s = k_{\mathrm{B}}TC\omega_0^2\left[1 - \frac{C}{4L_{\mathrm{p\_ds}}}\left(\frac{k_{\mathrm{B}}T}{L_{\mathrm{p\_ds}}F}\right)^{1/2}\right], \tag{12}$$

where $\omega_0 = 2\pi/(3.6\text{ nm})$ is the conversion between natural angle of rotation and contour length, $C = 100$ nm the intrinsic twist persistence length(Sheinin and Wang 2009), and L_0 contour length of the dsDNA. This expression is valid until the onset of a phase transition from B-DNA to another phase. The force dependence of c_s also implies that twist influences DNA extension. The force-extension relation of the dsDNA shown in Eq. (2) needs to be slightly revised(Marko 2007; Sheinin and Wang 2009) to consider contribution from twist.

For the torsionally constrained trunk in the Y structure, σ and L_0 are directly coupled via the number of base pairs unzipped n: $\sigma = \frac{n}{n_{\text{tr}}-n}$, and $L_0 = (n_{\text{tr}} - n)L_{0\_\text{ds}}$.

Therefore,

$$G_{\text{twist}}(F_{\text{tr}}, \sigma, L_0) = G_{\text{twist}}(F_{\text{tr}}, n). \tag{13}$$

The free energy of the Y structure after taking into consideration the torsion in the trunk is:

$$G_2(n; x_{\text{a}}, F_{\text{tr}}) = G_1(n; x_{\text{a}}, F_{\text{tr}}) + G_{\text{twist}}(F_{\text{tr}}, n). \tag{14}$$

This additional torsional energy term is very significant as it predicts a steep increase in torsional energy even when a small number of base pairs are unzipped. In addition, to remain in the region of B-DNA, σ must be small (< 0.04 at 2 pN of trunk force) after which the existence of plectonemes must be considered(Forth et al. 2008). This puts a limit on the number of base pairs that can be unzipped before plectonemes begin to form in the trunk DNA. For a 4 kb trunk, this is only about ~ 160 bp.

Once $G_2(n; x_a, F_{tr})$ is determined, the arm force and the number of base pairs unzipped can be found using a partition function of the form in Eqs. (7) and (8) by replacing $G(n; x_a, z_a)$ with $G_2(n; x_a, F_{tr})$. As shown in **Fig. 14**, the force required to unzip torsionally constrained trunk DNA significantly differs from that for unzipping torsionally relaxed trunk DNA (**Fig. 13**). The steep force rise is a strong signature of torsional constraint and is readily identifiable in single molecule experiments.

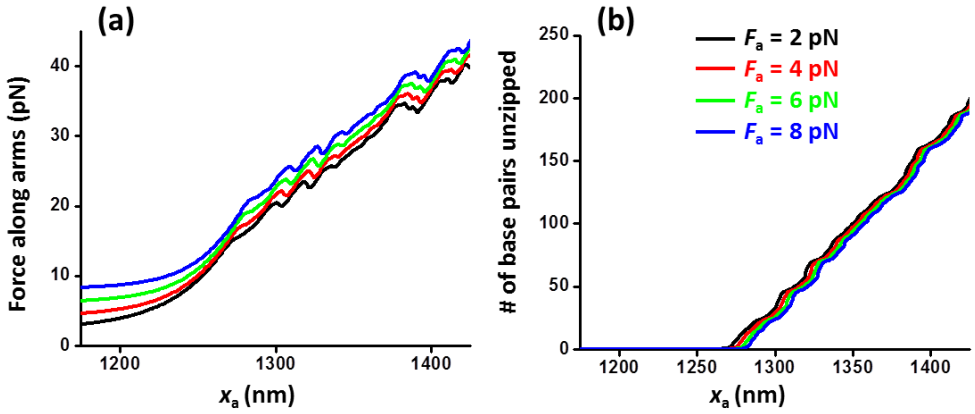

Figure 14. Arm forces under a torsionally constrained trunk of the Y structure. Results are shown for several values of the trunk forces.

(a) Force along arms versus x_a.

(b) Number (#) of base pairs unzipped versus x_a.

The Y structure under constant forces

To gain an intuitive understanding of the unzipping force for the Y structure, we consider unzipping of a homopolymeric Y structure under constant forces in all three branches. For simplicity, we consider a symmetric Y structure initially consisting of no dsDNA arms (i.e., $n_{\mathrm{arm}} = 0$) and a trunk of n_{tr} base pairs of dsDNA (**Fig. 15**). The force in each arm is held constant with a magnitude F at an angle θ with respect to the z axis. The trunk force is thus also held constant with a magnitude $F_{\mathrm{tr}} = 2F\cos\theta$. For a homopolymeric DNA trunk, each base has the same magnitude of base pairing energy (E_{bp}). The free energy of the system is thus composed of the free energy increase due to the loss of base pairing of the first n base pairs unzipped and the DNA stretching energy in all three branches under constant forces:

$$G_3(n;F,\theta) = n\,E_{\mathrm{bp}} - 2n\int_0^F s_{\mathrm{ss}}(F')dF' - (n_{\mathrm{tr}} - n)\left(\int_0^{2F\cos\theta} s_{\mathrm{ds}}(F')dF'\right). \tag{15}$$

We will eliminate the term that does not depend on n because this term does not contribute to partitioning of the states:

$$\Delta G_3(n;F,\theta) = n\,E_{\mathrm{bp}} - 2n\int_0^F s_{\mathrm{ss}}(F')dF' + n\int_0^{2F\cos\theta} s_{\mathrm{ds}}(F')dF'$$

$$= n\left[E_{\mathrm{bp}} - 2\int_0^F s_{\mathrm{ss}}(F')dF' + \int_0^{2F\cos\theta} s_{\mathrm{ds}}(F')dF'\right]. \tag{16}$$

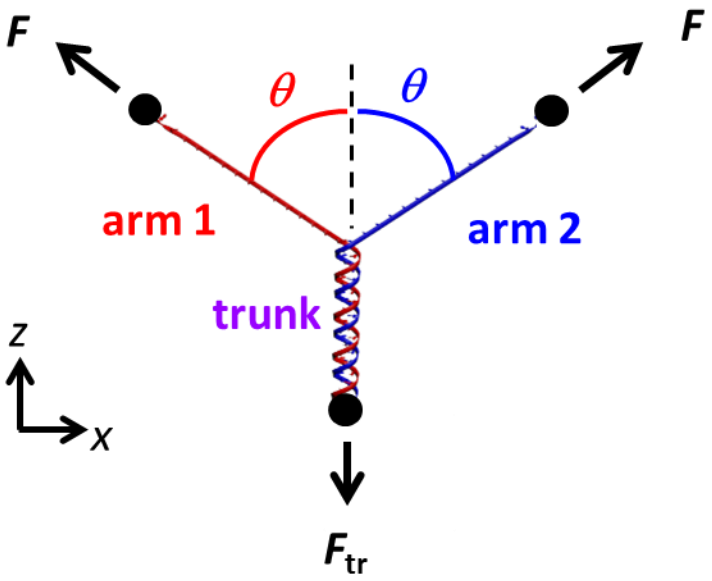

Figure 15. Geometry of the Y structure under constant forces in all three branches. The Y structure is confined to the *xz* plane and is symmetric about the trunk. Each arm consists of ssDNA held at a constant force of magnitude F at angle θ with respect to the trunk.

Therefore, the presence of a trunk force term (the last term) which has the same sign as the base-pairing energy indicates stabilization of the trunk relative to the 1D unzipping case.

When $\theta = \frac{\pi}{2}$, this corresponds to 1D unzipping which has been shown to have a critical transition from DNA being fully base paired to fully unzipped as force in increased above a critical value(Lubensky and Nelson 2002; Danilowicz et al. 2003). Therefore, we expect a similar transition to occur for unzipping of the Y structure. Indeed, since $\Delta G_3(n; F, \theta)$ is proportional to n, the minimum free energy state corresponds to either $n = 0$ (trunk DNA remains fully double stranded) when $F < F_c$ or $n = n_{tr}$ (trunk is fully unzipped) when $F > F_c$. At the critical force $F = F_c$, $\Delta G_3(n; F, \theta)$ is independent of n and thus the fork fluctuates between these extremes. As shown in **Fig. 16**, the calculation is valid for trunk forces < 65 pN, at which the trunk undergoes a B-S transition(King et al. 2013; Zhang et al. 2013). As θ increases towards $\theta = \frac{\pi}{2}$ (1D unzipping limit), F_c decreases while its z component $F_{c,z}$ decreases more steeply. Consequently, F_c increases with an increase in $F_{c,tr}\left(= 2F_{c,z}\right)$. $F_{c,x}$, the x component F_c, is greater than the 1D unzipping force over the valid range of the theory.

We will specifically evaluate how F_c and $F_{c,x}$ vary with θ as θ decrease from $\theta = \pi/2$ (1D unzipping). The first derivative of $F_c(\theta)$ with respect to θ is:

$$\frac{dF_c}{d\theta} = \frac{\partial \Delta G_3}{\partial \theta} \Big/ \frac{\partial \Delta G_3}{\partial F_c} = \frac{2F_c \sin\theta s_{ds}(2F_c \cos\theta)}{-2s_{ss}(F_c)+2\cos\theta s_{ds}(2F_c \cos\theta)}. \quad (17)$$

This gives $\left.\frac{dF_c}{d\theta}\right|_{\theta=\pi/2} = 0$. The second derivative of $F_c(\theta)$ with respect to θ at $\theta = \frac{\pi}{2}$ is:

$$\left.\frac{d^2F_c}{d\theta^2}\right|_{\theta=\pi/2} = \frac{2{F_c}^2}{s_{ss}(F_c)} \left.\frac{ds_{ds}}{dF}\right|_{F=0} > 0. \quad (18)$$

Since $\left.\frac{d^2F_c}{d\theta^2}\right|_{\theta=\pi/2}$ is always positive, F_c must increase as force is applied to the trunk.

Next we examine the x component of the force $F_{c,x}$.

$$\left.\frac{dF_{c,x}}{d\theta}\right|_{\theta=\pi/2} = 0 \quad (19)$$

$$\left.\frac{d^2F_{c,x}}{d\theta^2}\right|_{\theta=\pi/2} = \left.\frac{d^2F_c}{d\theta^2}\right|_{\theta=\pi/2} - F_c = \frac{2{F_c}^2}{s_{ss}(F_c)} \left.\frac{ds_{ds}}{dF}\right|_{F=0} - F_c \quad (20)$$

Since $\left.\frac{dF}{ds_{ds}}\right|_{F=0} < \frac{2F_c}{s_{ss}(F_c)}$ because dsDNA has a low stiffness under a small force, $\left.\frac{d^2F_{c,x}}{d\theta^2}\right|_{\theta=\pi/2} > 0$.

Therefore, $F_{c,x}$ will also increase as the trunk is extended.

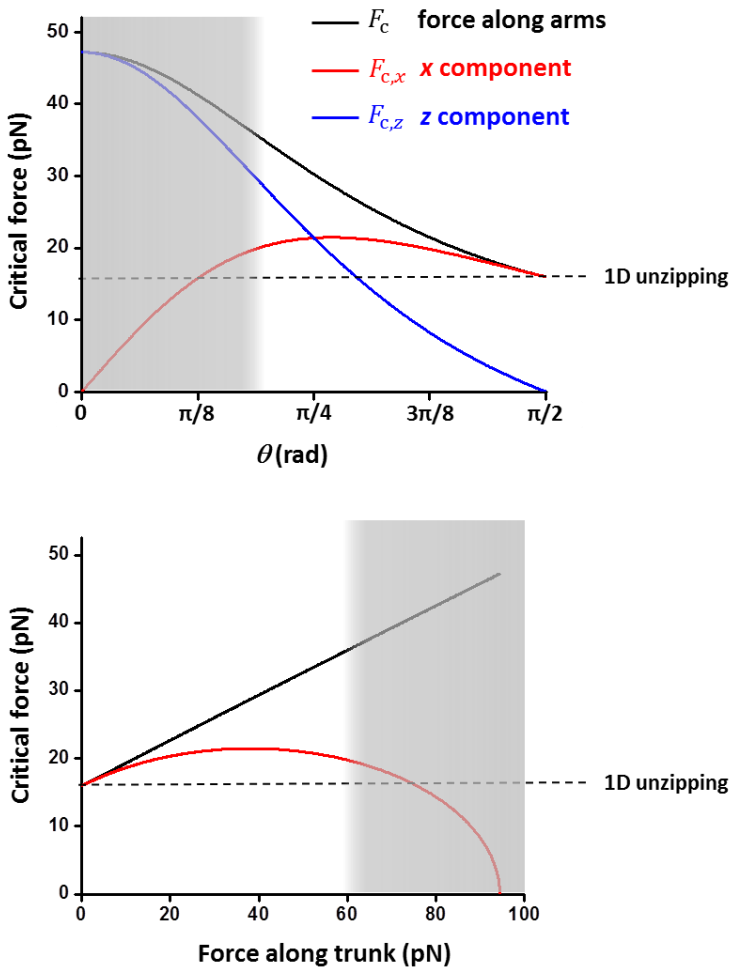

Figure 16. Critical force of the Y structure under constant force. For this calculation, the homopolymeric DNA trunk is assumed to a base pairing energy $E_{\mathrm{bp}} = 2.4\ k_{\mathrm{B}}T$. (Top panel) The critical force, at which the Y structure unzips, is plotted as a function of the angle of the applied force. $\theta = \pi/2$ corresponds to 1D unzipping where there is no force on the trunk. As trunk force increases above 65 pN, trunk DNA is expected to undergo a B-S phase transition (shaded region) which our theory does not consider. (Bottom panel) The critical force is plotted as a function of the force along the trunk for a more direct comparison with our experimental results.

Y structure in conjunction with fluorescence

While unzipping is able to accurately locate a protein already bound to dsDNA, it cannot provide real-time information on protein binding, nor the location of a protein on ssDNA. Fluorescence visualization thus complements unzipping. We have integrated Y structure manipulation with fluorescence in order to combine the high resolution mapping by unzipping with direct visualization by fluorescence.

In order to demonstrate this integration, we first formed a paused transcription elongation complex (TEC) on the DNA trunk and then labelled the RNA polymerase (RNAP) with a quantum dot (**Fig. 17a**). TEC was formed on the trunk DNA following a protocol similar to that previously established(Schafer et al. 1991; Yin et al. 1995). Briefly, the 3.7 kbp trunk DNA (10 nM) was incubated with *E. coli* RNA polymerase (100 nM) for 30 minutes at 37 °C in the transcription buffer (25 mM Tris-Cl pH 8.0, 100 mM KCl, 4 mM $MgCl_2$, 1 mM DTT, 0.4 mg/mL BSA, 7.5% glycerol, 50 μM ATP/GTP/CTP, 100 μM ApU, 1U/μL SUPERase-In). The resulting trunk contained a transcription elongation complex paused at +20 bp from the promoter. The trunk DNA was then ligated to the short Y-arm.

The RNAP was fluorescently labeled with quantum dots using standard antibody labeling techniques which has been demonstrated not to interfere with protein-DNA binding(Wang et al. 2008). Briefly, single molecule Y-structure tethers were formed in a microscope flow cell. Purified HA-tagged RNAP(Bai et al. 2007; Jin et al. 2010)

as labeled with primary antibody to HA expressed in mouse (Covance). Excess antibodies were washed out of the chamber PBS. Quantum dots coated with secondary antibodies (Invitrogen A-10195) were flowed in to bind to the primary antibodies. Excess quantum dots were washed out of the chamber PBS.

We then unzipped through the TEC, while simultaneously acquiring optical trapping data, bright field images, and fluorescence images in real time (**Fig. 17b**). The trapping data permitted the determination of the exact geometry of the Y structure DNA, eliminating the need to directly visualize the Y structure. The bright field images showed the locations of the two trapped microspheres and fluorescence images showed the locations of the RNAP. Correlation of the fluorescence images with the unzipping data shows that the TEC was located at the junction when the force rise was detected (**Fig 17c**).

Figure 17. Simultaneous stretching, unzipping, and fluorescence.

(**a**) A cartoon illustrating the experimental configuration. The Y structure contained two arms of different lengths in order to facilitate differentiation of the two arms, and a trunk with a paused transcription elongation complex (TEC) formed with an HA-tagged *E. coli* RNAP. The RNAP was subsequently labelled by anti-HA, which was then labeled by secondary-antibody coated quantum dots. The trunk containing the RNAP was subsequently unzipped under X pN of force along the trunk.

(**b**) Snapshots of images during unzipping through a trunk containing an RNAP in head-on collision with unzipping. Fluorescence images (red) showed the locations of RNAP and bright field images (green) showed the locations of the two trapped microspheres. Optical trapping measurements provided the lengths and geometry of the three branches in the Y structure (white lines).

(**c**) Measured force along arms versus number of base pairs unzipped for the example shown in (**b**). The red dashed line indicates the expected active site location of the TEC. Arrows correlate the time points for images shown in (**b**). At time point 2, the TEC was disrupted.

(**d**) Histograms showing RNAP fates upon unzipping. The locations of RNAP after either co-directional or head-on collisions with unzipping were determined by making multiple measurements such as those shown in (**b**) and (**c**).

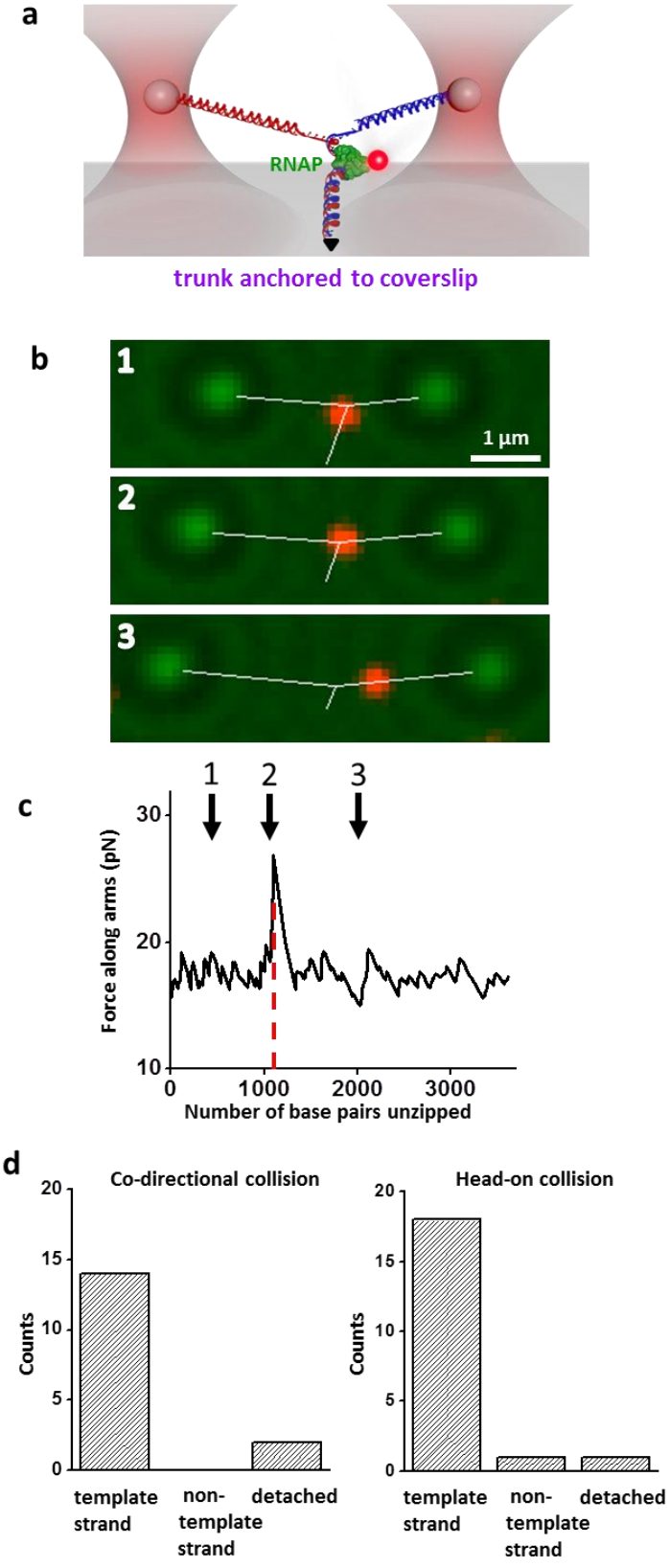
a
RNAP
trunk anchored to coverslip
b
1
2
3
1 µm
c
1
2
3
30
20
10
Force along arms (pN)
0
1000
2000
3000
Number of base pairs unzipped
d
Co-directional collision
Head-on collision
Counts
20
15
10
5
0
template strand
non-template strand
detached

Interestingly, fluorescence visualization of the RNAP revealed that, after the DNA was unzipped through the TEC, the RNAP almost exclusively remained bound to the template strand of the DNA (Methods). This occurred regardless of whether the unzipping fork collided with RNAP co-directionally (in the same direction as transcription) or head-on (in the opposite direction to transcription) (**Fig. 17d**). This finding has significant implications for replication-transcription collision (see Discussion below).

We also show that unzipping provides accurate measurements of the detailed interaction of RNAP with the trunk. When the unzipping fork encountered the RNAP paused at 20 nt after the transcription start site (+20 site), we found that RNAP significantly altered the unzipping force, compared to that of naked DNA (**Fig. 18**). For a co-directional collision, a force reduction appeared 24 ± 8 nt (mean ± SD) upstream of the +20 site, which we interpret as the fork beginning to interact with the transcription bubble (**See below**). This was followed by a dramatic increase in unzipping force at the +20 site (± 4 nt), which we interpret as the fork encountering the downstream dsDNA that was tightly clamped by the RNAP. These findings from the Y-structure are consistent with our previous findings using 1D unzipping(Jin et al. 2010). For a head-on collision, a dramatic force rise occurred at 14 ± 3 bp downstream of the +20 site, which we interpret as the fork encountering the far downstream dsDNA that was tightly clamped by the RNAP. These measurements compare well with TEC structure determination from previous biochemical studies(Lee and Landick 1992; Zaychikov et al. 1995). It is worth noting that a paused

TEC at this +20 site is known to backtrack(Jin et al. 2010) and should contribute to the measured heterogeneity in the TEC population. Thus, in addition to locating the TEC to near base pair accuracy, these measurements mapped out detailed interactions and their strengths within the TEC.

Figure 18. Mapping the structure of the transcription elongation complex (TEC).

(**a**) Unzipping DNA through a TEC from either co-directional collision (top panel) or head-on collision (bottom panel) directions. The TEC was paused at +20 bp from the start site and the trunk was held at 4 pN of force. The theoretical predictions of the unzipping force of naked DNA are also shown for comparison (grey). Three characteristic locations are highlighted. In the co-directional unzipping direction, the onset of the force drop indicates the presence of the transcription bubble, and the subsequent force rise corresponds to the end of the transcription bubble and the beginning of the dsDNA clamped by RNAP. In the head-on unzipping direction, a force rise corresponds to the onset of the RNAP interaction with the downstream dsDNA.

(**b**) A cartoon of the TEC indicating the locations of the three detectable features discussed above.

(**c**) An RNAP-DNA interaction map of the TEC. Three histograms were obtained by pooling a number of measurements such as those shown in (**a**). They show the locations for the onset of the force drop (red) and the force rise peak (black) in the co-directional unzipping direction, and the force rise peak (green) in the head-on unzipping direction relative to the transcription start site (+1 bp corresponds to the transcription start site). The mean position of each histogram is indicated by a dashed line. The distance between the red and black dashed lines is ~ 25 bp which is an overestimate of the actual transcription bubble size. The distance between the green and black lines is ~ 14 bp and provides the length of the downstream dsDNA region tightly clamped by RNAP.

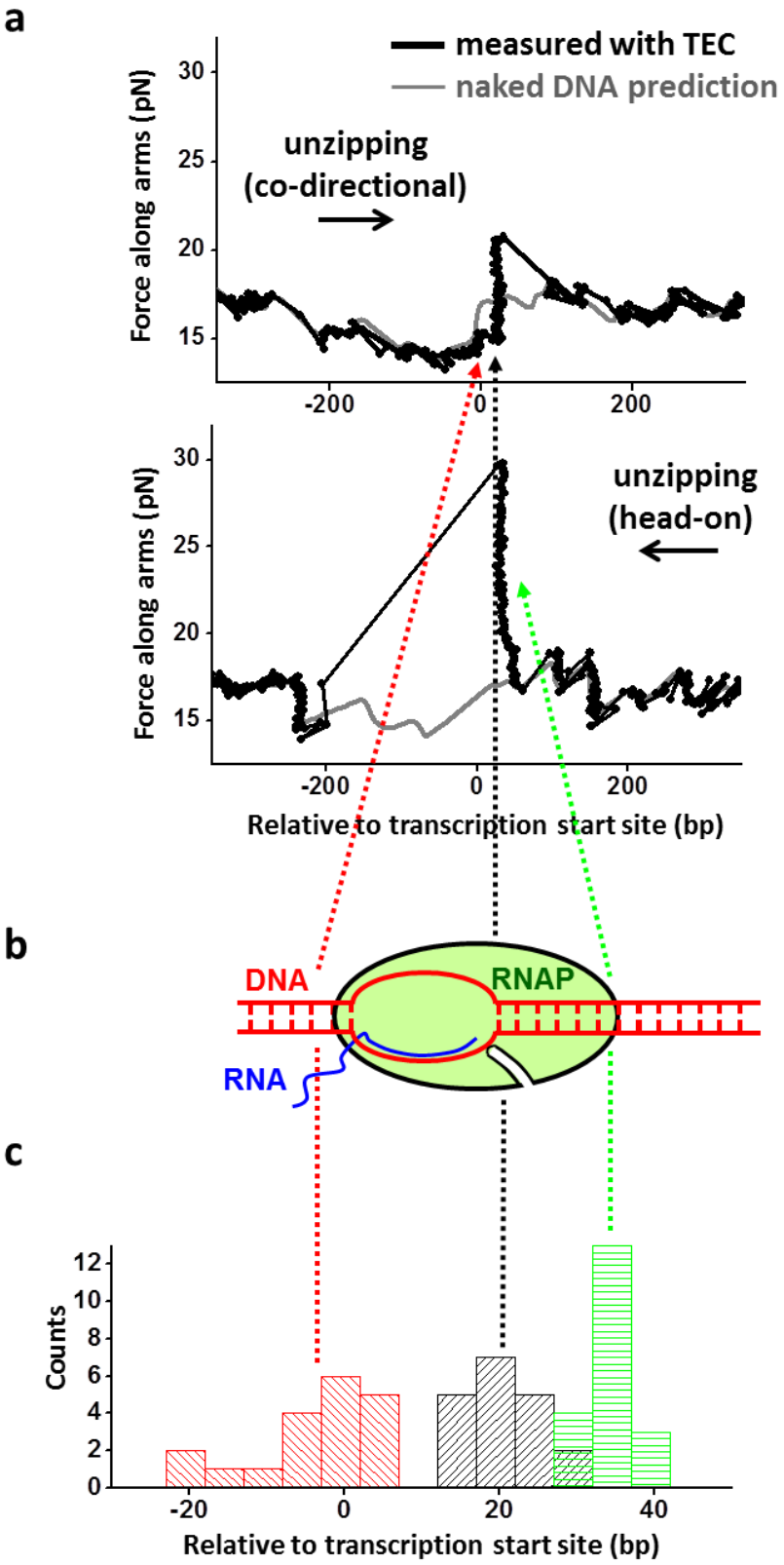
a
measured with TEC
naked DNA prediction
unzipping
(co-directional)
Force along arms (pN)
30
25
20
15
-200
0
200
unzipping
(head-on)
Relative to transcription start site (bp)
b
DNA
RNAP
RNA
c
Counts
12
10
8
6
4
2
0
-20
0
20
40
Relative to transcription start site (bp)

We found that when DNA containing a TEC was unzipped co-directionally with the direction of transcription, a force drop occurred a few base pairs before the expected location of the edge of the transcription bubble. We interpret this as a result of thermal fluctuations of the unzipping fork. As DNA is unzipped, the unzipping fork is expected to fluctuate among multiple energy states, at rates much faster than the unzipping speed. Therefore, the measured fork position represents the mean value for the fork position(Bockelmann et al. 1997; Bockelmann et al. 1998). The extent of fluctuations is DNA sequence-dependent but is of the order of 5-10 base pairs (**Fig. 19**). As the fork approaches a DNA bubble, the fork's excursions away from the mean may encounter the DNA bubble. At this point, the fork will immediately open the entire bubble and become trapped in the much lower energy open state. Thus, the location of the start of a bubble will always be detected closer to the unzipping fork than the bubble's actual edge. The extent of the shift will be related to the local DNA sequence, the temperature, and the rate of unzipping. By contrast, the location of the end of the bubble can be determined with much more certainty. Therefore, when the region of force drop is used to determine the bubble size, the size is always over-estimated.

Therefore, the combination of unzipping with fluorescence allowed us to 1) visualize RNAP presence on the trunk prior to unzipping, 2) accurately determine its location and its TEC structure on the trunk upon unzipping, and, 3) visualize its presence on the ssDNA after unzipping.

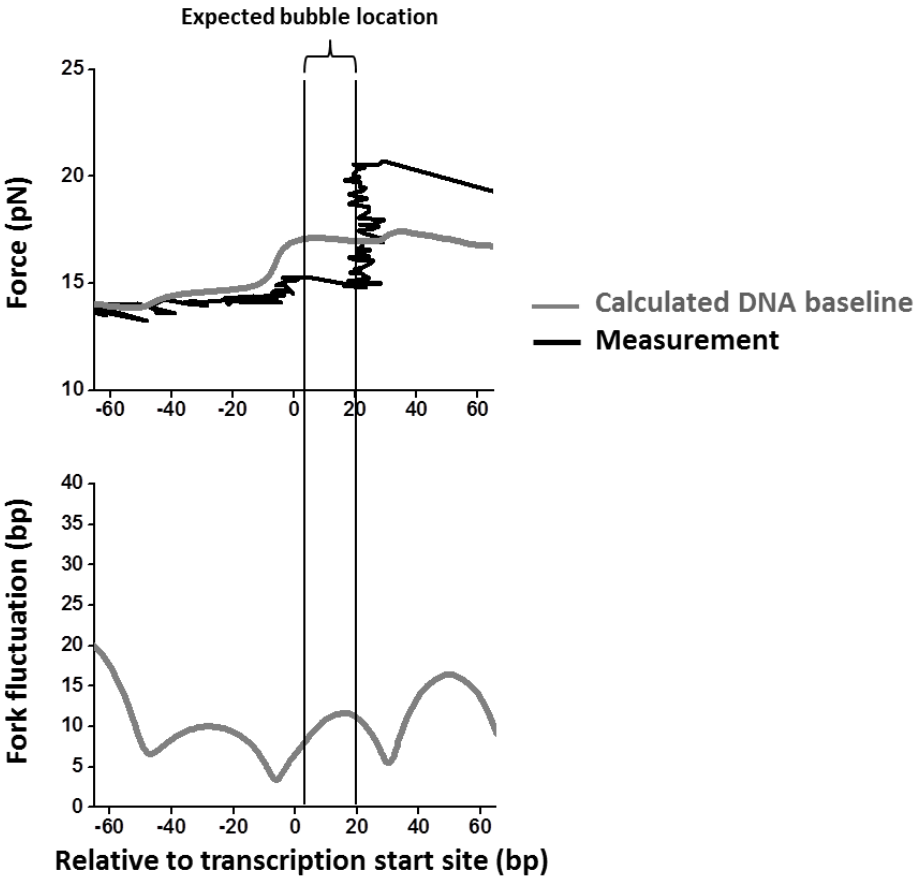

Figure 19. Fluctuations of the unzipping fork in the presence of a transcription bubble. (upper) Measured unzipping force in the presence of a paused transcription elongation complex (TEC) (black) compared with the calculated unzipping force in the absence of a TEC (grey). (lower) Calculated fork fluctuations (standard deviation of the number of base pairs unzipped) near the paused TEC. All calculations were performed for a constant trunk force of 4 pN.

Discussion

Previous single molecule studies have been restricted to measuring physical quantities along one dimension, limiting the examination of complex biomolecular systems. Our novel Y structure assay measures forces and extensions on DNA in two dimensions, can impose torsional constraint on DNA, and is compatible with fluorescence.

Although the focus of this report is on methodology development, a number of results already have important implications for processes that take place on DNA. We found that the unzipping force increased when tension was present in the dsDNA trunk and a much more dramatic increase occurred when the trunk was torsionally constrained. *In vivo*, DNA is expected to be under some tension and torsion generated by motor proteins and topological or geometrical constraints. Thus, processes which must enzymatically unwind (or unzip) DNA, such as replication and possibly transcription, will encounter increased resistance to translocation over what would be expected with relaxed DNA. In particular, even moderate torsional constraint could create a substantial barrier for unwinding DNA. Thus, this new assay provides a method to study the interplay of DNA mechanical properties and the interactions of proteins and DNA.

Another important aspect of this single molecule assay is its ability to determine the locations of proteins after they dissociate from the template. We found that when the unzipping fork disrupted the TEC, RNAP primarily remained on the template strand

for both co-directional and head-on collisions. Our experimental approach is reminiscent of replication and transcription collisions where a replisome encounters transcription machinery(Pomerantz and O'Donnell 2010). Indeed, our findings coincide with previous studies which suggest that RNAP stays associated with the template DNA and remains active after the passage of a replication fork during co-directional and head-on collisions of replication and transcription. The Y structure is ideally suited to investigate these collisions.

Although we demonstrate the Y structure assay with three branches composed of DNA, each branch may be composed of any combination of single stranded or double stranded DNA or RNA. The three-way junction can also be extended to multiple junctions, each of which may be directly measured in 3D.

The addition of new measurement axes allows for a plethora of interesting experimental possibilities. The Y structure assay allows a new generation of single molecule studies focused on characterizing interactions of multiple proteins during complex processes such as transcription and replication. The ability to combine stretching, twisting, unzipping and fluorescent imaging in a single assay provides a versatile system for measuring the complex geometries and protein interactions during these processes.

Acknowledgements

We thank members of the Wang lab for critical reading of the manuscript. We especially thank Dr. R.M. Fulbright for purification of RNA polymerase. We wish to acknowledge graduate traineeship support to J.I. from Cornell University's Molecular Biophysics Training Grant (T32GM008267), postdoctoral support to R.A.F. from the American Cancer Society (125126-PF-13-205-01-DMC), Support to J.P.S from National Science Foundation grant (DMR 1312160), and support to M.D.W. from the National Institutes of Health grant (GM059849) and National Science Foundation grant (MCB-0820293).

References

Adelman, K., Yuzenkova, J., La Porta, A., Zenkin, N., Lee, J., Lis, J. T., Borukhov, S., Wang, M. D. and Severinov, K. (2004). "Molecular mechanism of transcription inhibition by peptide antibiotic Microcin J25." Mol Cell **14**(6): 753-762.

Bai, L., Fulbright, R. M. and Wang, M. D. (2007). "Mechanochemical kinetics of transcription elongation." Phys Rev Lett **98**(6): 068103.

Bennink, M. L., Leuba, S. H., Leno, G. H., Zlatanova, J., de Grooth, B. G. and Greve, J. (2001). "Unfolding individual nucleosomes by stretching single chromatin fibers with optical tweezers." Nat Struct Biol **8**(7): 606-610.

Bockelmann, U., Essevaz-Roulet, B. and Heslot, F. (1998). "DNA strand separation studied by single molecule force measurements." Physical Review E **58**(2): 2386-2394.

Bockelmann, U., EssevazRoulet, B. and Heslot, F. (1997). "Molecular stick-slip motion revealed by opening DNA with piconewton forces." Physical Review Letters **79**(22): 4489-4492.

Bockelmann, U., Thomen, P., Essevaz-Roulet, B., Viasnoff, V. and Heslot, F. (2002). "Unzipping DNA with optical tweezers: high sequence sensitivity and force flips." Biophys J **82**(3): 1537-1553.

Brower-Toland, B., Wacker, D. A., Fulbright, R. M., Lis, J. T., Kraus, W. L. and Wang, M. D. (2005). "Specific contributions of histone tails and their acetylation to the mechanical stability of nucleosomes." J Mol Biol **346**(1): 135-146.

Brower-Toland, B. D., Smith, C. L., Yeh, R. C., Lis, J. T., Peterson, C. L. and Wang, M. D. (2002). "Mechanical disruption of individual nucleosomes reveals a reversible multistage release of DNA." Proc Natl Acad Sci U S A **99**(4): 1960-1965.

Candelli, A., Hoekstra, T. P., Farge, G., Gross, P., Peterman, E. J. and Wuite, G. J. (2013). "A toolbox for generating single-stranded DNA in optical tweezers experiments." Biopolymers **99**(9): 611-620.

Comstock, M. J., Ha, T. and Chemla, Y. R. (2011). "Ultrahigh-resolution optical trap with single-fluorophore sensitivity." Nat Methods **8**(4): 335-340.

Cui, Y. and Bustamante, C. (2000). "Pulling a single chromatin fiber reveals the forces that maintain its higher-order structure." Proc Natl Acad Sci U S A **97**(1): 127-132.

Dame, R. T., Noom, M. C. and Wuite, G. J. (2006). "Bacterial chromatin organization by H-NS protein unravelled using dual DNA manipulation." Nature **444**(7117): 387-390.

Daniels, B. C., Forth, S., Sheinin, M. Y., Wang, M. D. and Sethna, J. P. (2009). "Discontinuities at the DNA supercoiling transition." Phys Rev E Stat Nonlin Soft Matter Phys **80**(4 Pt 1): 040901.

Danilowicz, C., Coljee, V. W., Bouzigues, C., Lubensky, D. K., Nelson, D. R. and Prentiss, M. (2003). "DNA unzipped under a constant force exhibits multiple metastable intermediates." Proc Natl Acad Sci U S A **100**(4): 1694-1699.

Dessinges, M. N., Maier, B., Zhang, Y., Peliti, M., Bensimon, D. and Croquette, V. (2002). "Stretching single stranded DNA, a model polyelectrolyte." Phys Rev Lett **89**(24): 248102.

Deufel, C., Forth, S., Simmons, C. R., Dejgosha, S. and Wang, M. D. (2007). "Nanofabricated quartz cylinders for angular trapping: DNA supercoiling torque detection." Nat Methods **4**(3): 223-225.

Deufel, C. and Wang, M. D. (2006). "Detection of forces and displacements along the axial direction in an optical trap." Biophys J **90**(2): 657-667.

Dijk, M. A., Kapitein, L. C., Mameren, J., Schmidt, C. F. and Peterman, E. J. (2004). "Combining optical trapping and single-molecule fluorescence spectroscopy: enhanced photobleaching of fluorophores." J Phys Chem B **108**(20): 6479-6484.

Dumont, S., Cheng, W., Serebrov, V., Beran, R. K., Tinoco, I., Jr., Pyle, A. M. and Bustamante, C. (2006). "RNA translocation and unwinding mechanism of HCV NS3 helicase and its coordination by ATP." Nature **439**(7072): 105-108.

Forget, A. L. and Kowalczykowski, S. C. (2012). "Single-molecule imaging of DNA pairing by RecA reveals a three-dimensional homology search." Nature **482**(7385): 423-427.

Forth, S., Deufel, C., Sheinin, M. Y., Daniels, B., Sethna, J. P. and Wang, M. D. (2008). "Abrupt buckling transition observed during the plectoneme formation of individual DNA molecules." Phys Rev Lett **100**(14): 148301.

Forth, S., Sheinin, M. Y., Inman, J. and Wang, M. D. (2013). "Torque measurement at the single-molecule level." Annu Rev Biophys **42**: 583-604.

Galletto, R., Amitani, I., Baskin, R. J. and Kowalczykowski, S. C. (2006). "Direct observation of individual RecA filaments assembling on single DNA molecules." Nature **443**(7113): 875-878.

Gemmen, G. J., Sim, R., Haushalter, K. A., Ke, P. C., Kadonaga, J. T. and Smith, D. E. (2005). "Forced unraveling of nucleosomes assembled on heterogeneous DNA using core histones, NAP-1, and ACF." J Mol Biol **351**(1): 89-99.

Gross, P., Laurens, N., Oddershede, L. B., Bockelmann, U., Peterman, E. J. G. and Wuite, G. J. L. (2011). "Quantifying how DNA stretches, melts and changes twist under tension." Nature Physics **7**(9): 731-736.

Hall, M. A., Shundrovsky, A., Bai, L., Fulbright, R. M., Lis, J. T. and Wang, M. D. (2009). "High-resolution dynamic mapping of histone-DNA interactions in a nucleosome." Nat Struct Mol Biol **16**(2): 124-129.

Hegner, M., Smith, S. B. and Bustamante, C. (1999). "Polymerization and mechanical properties of single RecA-DNA filaments." Proc Natl Acad Sci U S A **96**(18): 10109-10114.

Heller, I., Sitters, G., Broekmans, O. D., Farge, G., Menges, C., Wende, W., Hell, S. W., Peterman, E. J. and Wuite, G. J. (2013). "STED nanoscopy combined with optical tweezers reveals protein dynamics on densely covered DNA." Nat Methods **10**(9): 910-916.

Hohng, S., Zhou, R., Nahas, M. K., Yu, J., Schulten, K., Lilley, D. M. and Ha, T. (2007). "Fluorescence-force spectroscopy maps two-dimensional reaction landscape of the holliday junction." Science **318**(5848): 279-283.

Huguet, J. M., Bizarro, C. V., Forns, N., Smith, S. B., Bustamante, C. and Ritort, F. (2010). "Single-molecule derivation of salt dependent base-pair free energies in DNA." Proc Natl Acad Sci U S A **107**(35): 15431-15436.

Ibarra, B., Chemla, Y. R., Plyasunov, S., Smith, S. B., Lazaro, J. M., Salas, M. and Bustamante, C. (2009). "Proofreading dynamics of a processive DNA polymerase." EMBO J **28**(18): 2794-2802.

Ishijima, A., Kojima, H., Funatsu, T., Tokunaga, M., Higuchi, H., Tanaka, H. and Yanagida, T. (1998). "Simultaneous observation of individual ATPase and mechanical events by a single myosin molecule during interaction with actin." Cell **92**(2): 161-171.

Jin, J., Bai, L., Johnson, D. S., Fulbright, R. M., Kireeva, M. L., Kashlev, M. and Wang, M. D. (2010). "Synergistic action of RNA polymerases in overcoming the nucleosomal barrier." Nat Struct Mol Biol **17**(6): 745-752.

Johnson, D. S., Bai, L., Smith, B. Y., Patel, S. S. and Wang, M. D. (2007). "Single-molecule studies reveal dynamics of DNA unwinding by the ring-shaped T7 helicase." Cell **129**(7): 1299-1309.

King, G. A., Gross, P., Bockelmann, U., Modesti, M., Wuite, G. J. and Peterman, E. J. (2013). "Revealing the competition between peeled ssDNA, melting bubbles, and S-DNA during DNA overstretching using fluorescence microscopy." Proc Natl Acad Sci U S A **110**(10): 3859-3864.

Koch, S. J., Shundrovsky, A., Jantzen, B. C. and Wang, M. D. (2002). "Probing protein-DNA interactions by unzipping a single DNA double helix." Biophys J **83**(2): 1098-1105.

Koch, S. J. and Wang, M. D. (2003). "Dynamic force spectroscopy of protein-DNA interactions by unzipping DNA." Phys Rev Lett **91**(2): 028103.

Koster, D. A., Crut, A., Shuman, S., Bjornsti, M. A. and Dekker, N. H. (2010). "Cellular strategies for regulating DNA supercoiling: a single-molecule perspective." Cell **142**(4): 519-530.

Lang, M. J., Fordyce, P. M. and Block, S. M. (2003). "Combined optical trapping and single-molecule fluorescence." J Biol **2**(1): 6.

Lang, M. J., Fordyce, P. M., Engh, A. M., Neuman, K. C. and Block, S. M. (2004). "Simultaneous, coincident optical trapping and single-molecule fluorescence." Nat Methods **1**(2): 133-139.

Lee, D. N. and Landick, R. (1992). "Structure of RNA and DNA chains in paused transcription complexes containing Escherichia coli RNA polymerase." J Mol Biol **228**(3): 759-777.

Li, M. and Wang, M. D. (2012). "Unzipping single DNA molecules to study nucleosome structure and dynamics." Methods Enzymol **513**: 29-58.

Lubensky, D. K. and Nelson, D. R. (2002). "Single molecule statistics and the polynucleotide unzipping transition." Phys Rev E Stat Nonlin Soft Matter Phys **65**(3 Pt 1): 031917.

Ma, J., Bai, L. and Wang, M. D. (2013). "Transcription under torsion." Science **340**(6140): 1580-1583.

Mangeol, P. and Bockelmann, U. (2008). "Interference and crosstalk in double optical tweezers using a single laser source." Review of Scientific Instruments **79**(8).

Marko, J. F. (2007). "Torque and dynamics of linking number relaxation in stretched supercoiled DNA." Phys Rev E Stat Nonlin Soft Matter Phys **76**(2 Pt 1): 021926.

Marko, J. F. and Siggia, E. D. (1995). "Stretching DNA." Macromolecules **28**(26): 8759-8770.

Mihardja, S., Spakowitz, A. J., Zhang, Y. and Bustamante, C. (2006). "Effect of force on mononucleosomal dynamics." Proc Natl Acad Sci U S A **103**(43): 15871-15876.

Moffitt, J. R., Chemla, Y. R., Izhaky, D. and Bustamante, C. (2006). "Differential detection of dual traps improves the spatial resolution of optical tweezers." Proc Natl Acad Sci U S A **103**(24): 9006-9011.

Noom, M. C., van den Broek, B., van Mameren, J. and Wuite, G. J. (2007). "Visualizing single DNA-bound proteins using DNA as a scanning probe." Nat Methods **4**(12): 1031-1036.

Pomerantz, R. T. and O'Donnell, M. (2010). "What happens when replication and transcription complexes collide?" Cell Cycle **9**(13): 2537-2543.

Schafer, D. A., Gelles, J., Sheetz, M. P. and Landick, R. (1991). "Transcription by single molecules of RNA polymerase observed by light microscopy." Nature **352**(6334): 444-448.

Sheinin, M. Y., Li, M., Soltani, M., Luger, K. and Wang, M. D. (2013). "Torque modulates nucleosome stability and facilitates H2A/H2B dimer loss." Nat Commun **4**: 2579.

Sheinin, M. Y. and Wang, M. D. (2009). "Twist-stretch coupling and phase transition during DNA supercoiling." Phys Chem Chem Phys **11**(24): 4800-4803.

Shundrovsky, A., Smith, C. L., Lis, J. T., Peterson, C. L. and Wang, M. D. (2006). "Probing SWI/SNF remodeling of the nucleosome by unzipping single DNA molecules." Nat Struct Mol Biol **13**(6): 549-554.

Smith, D. E., Tans, S. J., Smith, S. B., Grimes, S., Anderson, D. L. and Bustamante, C. (2001). "The bacteriophage straight phi29 portal motor can package DNA against a large internal force." Nature **413**(6857): 748-752.

Smith, S. B., Cui, Y. and Bustamante, C. (1996). "Overstretching B-DNA: the elastic response of individual double-stranded and single-stranded DNA molecules." Science **271**(5250): 795-799.

Sun, B., Johnson, D. S., Patel, G., Smith, B. Y., Pandey, M., Patel, S. S. and Wang, M. D. (2011). "ATP-induced helicase slippage reveals highly coordinated subunits." Nature **478**(7367): 132-135.

van Mameren, J., Modesti, M., Kanaar, R., Wyman, C., Peterman, E. J. and Wuite, G. J. (2009). "Counting RAD51 proteins disassembling from nucleoprotein filaments under tension." Nature **457**(7230): 745-748.

Wang, H., Tessmer, I., Croteau, D. L., Erie, D. A. and Van Houten, B. (2008). "Functional characterization and atomic force microscopy of a DNA repair protein conjugated to a quantum dot." Nano Lett **8**(6): 1631-1637.

Wang, M. D., Schnitzer, M. J., Yin, H., Landick, R., Gelles, J. and Block, S. M. (1998). "Force and velocity measured for single molecules of RNA polymerase." Science **282**(5390): 902-907.

Wang, M. D., Yin, H., Landick, R., Gelles, J. and Block, S. M. (1997). "Stretching DNA with optical tweezers." Biophys J **72**(3): 1335-1346.

Wuite, G. J., Smith, S. B., Young, M., Keller, D. and Bustamante, C. (2000). "Single-molecule studies of the effect of template tension on T7 DNA polymerase activity." Nature **404**(6773): 103-106.

Yin, H., Wang, M. D., Svoboda, K., Landick, R., Block, S. M. and Gelles, J. (1995). "Transcription against an applied force." Science **270**(5242): 1653-1657.

Zaychikov, E., Denissova, L. and Heumann, H. (1995). "Translocation of the Escherichia coli transcription complex observed in the registers 11 to 20: "jumping" of RNA polymerase and asymmetric expansion and contraction of the "transcription bubble"." Proc Natl Acad Sci U S A **92**(5): 1739-1743.

Zhang, X., Chen, H., Le, S., Rouzina, I., Doyle, P. S. and Yan, J. (2013). "Revealing the competition between peeled ssDNA, melting bubbles, and S-DNA during DNA

overstretching by single-molecule calorimetry." Proc Natl Acad Sci U S A **110**(10): 3865-3870.